HHS Public Access

Author manuscript

Exp Neurol. Author manuscript; available in PMC 2016 March 01.

Published in final edited form as:

Exp Neurol. 2015 March ; 265: 69–83. doi:10.1016/j.expneurol.2014.12.012.

Voltage-gated Ca^{++} entry promotes oligodendrocyte progenitor cells maturation and myelination in vitro

VT Cheli, **DA Santiago González**, **V Spreuer**, and **PM Paez**

Hunter James Kelly Research Institute, Department of Pharmacology and Toxicology, School of Medicine and Biomedical Sciences, SUNY, University at Buffalo. NYS Center of Excellence, 701 Ellicott St., Buffalo, New York 14203, USA

Abstract

We have previously shown that the expression of voltage-operated Ca^{++} channels (**VOCCs**) is highly regulated in the oligodendroglial lineage and is essential for proper oligodendrocyte progenitor cells (**OPCs**) migration. Here we assessed the role of VOCCs, in particular the L-type, in oligodendrocyte maturation. We used pharmacological treatments to activate or block voltage-gated Ca^{++} uptake and siRNAs to specifically knockdown the L-type VOCC in primary cultures of mouse OPCs. Activation of VOCCs by plasma membrane depolarization increased OPC morphological differentiation as well as the expression of mature oligodendrocyte markers. On the contrary, inhibition of L-type Ca^{++} channels significantly delayed OPC development. OPCs transfected with siRNAs for the Cav1.2 subunit that conducts L-type Ca^{++} currents showed reduce Ca^{++} influx by ~75% after plasma membrane depolarization, indicating that Cav1.2 is heavily involved in mediating voltage-operated Ca^{++} entry in OPCs. Cav1.2 knockdown induced a decrease in the proportion of oligodendrocytes that expressed myelin proteins, and an increase in cells that retained immature oligodendrocyte markers. Moreover, OPC proliferation, but not cell viability, was negatively affected after L-type Ca^{++} channel knockdown. Additionally, we have tested the ability of L-type VOCCs to facilitate axon-glial interaction during the first steps of myelin formation using an in vitro co-culture system of OPCs with cortical neurons. Unlike control OPCs, Cav1.2 deficient oligodendrocytes displayed a simple morphology, low levels of myelin proteins expression and appeared to be less capable of establishing contacts with neurites and axons. Together, this set of in vitro experiments characterizes the involvement of L-type VOCCs on OPCs maturation as well as the role played by these Ca^{++} channels during the early phases of myelination.

Keywords

oligodendrocyte; calcium influx; voltage-operated Ca^{++} channels; myelination

Correspondence to: Pablo M. Paez. Hunter James Kelly Research Institute, Department of Pharmacology and Toxicology, School of Medicine and Biomedical Sciences, SUNY at Buffalo. NYS Center of Excellence, 701 Ellicott St., Buffalo, New York 14203, USA. Tel: 716-881-7823; Fax: 716-849-6651; ppaez@buffalo.edu.

INTRODUCTION

Several studies have addressed the importance of Ca^{++} signaling in oligodendrocyte progenitor cell (**OPC**) differentiation and myelination (Soliven, 2001), as well as in processes extension and OPC migration (Simpson and Armstrong, 1999; Yoo et al., 1999), and in retraction of membrane sheets and cell death in mature mouse oligodendrocytes (Benjamins and Nedelkoska, 1996). Calcium influx across the oligodendrocyte plasma membrane can occur through a number of routes: (**1**) directly through a variety of ligand-operated channels, such as the α-adrenergic, P2Y, P2X and glutamate receptors (Kirchhoff and Kettenmann, 1992; Kastritsis and McCarthy, 1993; Patneau et al., 1994); (**2**) through voltage-operated Ca^{++} channels (**VOCCs**) activated in response to cell membrane depolarization, e.g. increased extracellular K^+; and (**3**) through other routes such as the opening of store-operated Ca^{++} channels in the membrane by the depletion of Ca^{++} stores in the endoplasmic reticulum (Alberdi et al., 2005; Belachew et al., 2000; Deitmer et al., 1998; Simpson et al., 1997). This work will focus on Ca^{++} influx mediated by VOCCs and the role that these Ca^{++} channels play during OPC development and the initial stages of myelination.

VOCCs are a vehicle for impulse generation and propagation in neurons and muscle cells, and thus, their expression in non-excitable cells was surprising. Six types of VOCCs (P/Q, N, L, R and T) have been classified on the basis of electrophysiological and pharmacological properties. Chen et al. (2000) found strong, transient expression of VOCCs in CNS white matter. The immunoreactivity appeared in glial cells along specific pathways of the brainstem, cerebellum and telencephalon. Ultrastructural analysis confirmed that VOCC immunoreactivity was located in oligodendroglial somata, projections, paranodal wraps and loose myelin sheaths (Chen et al., 2000). Electrophysiological recordings performed in our lab have identified low-voltage and high-voltage activated currents in corpus callosum OPCs. The low-voltage and high-voltage activated currents were found to possess the pharmacological and voltage-dependent properties of T-type and L-type VOCCs respectively (Fulton et al., 2010). These electrophysiological data are supported by calcium imaging data of primary OPC cultures and tissue slices depolarized with high K^+ (Paez et al., 2007; 2010).

We have shown that VOCCs affect many Ca^{++} dependent functions in OPCs as a consequence of their ability to modulate intracellular Ca^{++} concentrations. We have found that L-type VOCCs regulate extension/retraction of OPC processes (Paez et al., 2007). Additionally, we have provided direct evidence that L-type VOCC activation increases the amplitude of spontaneous Ca^{++} oscillations in the soma and in the leading process of migrating OPCs leading to an accelerated cell migration by promoting Ca^{++} dependent soma translocation and leading processes formation (Paez et al., 2009a). This mechanism illustrates a key role for VOCCs in the regulation of the rate of OPC migration through spontaneous Ca^{++} oscillations.

The overall goal of this work was to test the hypothesis that voltage-gated Ca^{++} entry promotes OPC maturation and the preliminary steps of myelination in vitro. We used different pharmacological treatments to activate or block voltage-gated Ca^{++} uptake and siRNAs to specifically knockdown the L-type VOCC in OPCs. We have found that VOCCs

are important regulators of the initial stages of myelination, from process extension to the initial contact with axons. This study will lead to new insight into the factors that govern OPC behavior and could lead to novel approaches to intervene in neurodegenerative diseases in which myelin is loss or damaged.

MATERIALS AND METHODS

Animal experimentation

All animals used in the present study were housed in the UB Division of Laboratory Animal Medicine vivarium, and procedures were approved by UB's Animal Care and Use Committee, and conducted in accordance with the guidelines in "Guide for the Care and Use of Laboratory Animals" from the National Institutes of Health.

Primary cultures of cortical OPCs

Primary cultures of cortical OPCs were prepared as described by Amur-Umarjee et al. (1993). First, cerebral hemispheres from 1 day old mice were mechanically dissociated and were plated on poly-D-lysine-coated flasks in Dulbecco´s modified Eagle´s medium and Ham´s F12 (1:1 v/v) (Invitrogen), containing 100μg/ml gentamycin and supplemented with 4mg/ml dextrose anhydrous, 3.75mg/ml HEPES buffer, 2.4mg/ml sodium bicarbonate and 10% fetal bovine serum (FBS) (Omega Scientific). After 24 hours the medium was changed and the cells were grown in DMEM/F12 supplemented with insulin (5μg/ml), human transferrin (50μg/ml), sodium selenite (30nM), d-Biotin (10mM), 0.1% BSA (Sigma), 1% FBS (Omega Scientific) and 1% horse serum (Omega Scientific). After 9 days, OPCs were purified from the mixed glial culture by the differential shaking and adhesion procedure of Suzumura et al., (1984) and allowed to grow on poly-D-lysine-coated coverslips in defined culture media (Agresti et al., 1996) plus PDGF (10ng/ml) and bFGF (10ng/ml) (Peprotech). OPCs were kept in mitogens (PDGF and bFGF) for 2 days and then induced to exit from the cell cycle and differentiate by switching the cells to a mitogen-free medium (mN2) (Oh et al., 2003) (Figure 1A). **mN2**: DMEM/F12 supplemented with d-glucose (4.5gm/l), insulin (5μg/ml), human transferrin (50μg/ml), sodium selenite (30nM), T_3 (15nM), d-Biotin (10mM), hydrocortisone (10nM), 0.1% BSA, 1% horse serum and 1% FBS.

siRNA knockdown of Cav1.2 and Cav1.3

Twenty-four hours after plating, the cells were transiently transfected with a combination of three different Stealth RNAi™ siRNA duplexes (Invitrogen) specific for Cav1.2 and Cav1.3 (see Table I for siRNA duplex sequences). Briefly, 6pmol of each siRNA duplex were mixed with Lipofectamine™ RNAiMAX (Invitrogen) and the mixture was added to 35mm Petri dishes containing 80% confluent OPCs. After transfection OPCs were further cultured for 24h in defined culture media (Agresti et al., 1996) plus PDGF (10ng/ml) and bFGF (10ng/ml) and then the cells were switched to a mitogen-free medium (mN2) to induce differentiation (Oh et al., 2003) (Figure 2A). Control cells were transfected with siRNA designed to minimize sequence homology to any known vertebrate transcript and with a similar GC content as our siRNAs. Additionally, following the transfection protocol described above, OPCs were treated with fluorescein-labeled dsRNA oligomers (BLOCK-iT™ Fluorescent Oligos, Invitrogen) to determine siRNA transfection efficiency.

Immunocytochemistry

Cells were stained with antibodies against several oligodendrocyte markers and examined by confocal microscopy. Briefly, the cells were rinsed in PBS and fixed in 4% buffered paraformaldehyde for 30min at room temperature. After rinsing in PBS, the cells were permeabilized with 0.1% Triton X-100 in PBS for 10min at room temperature and then processed for immunocytochemistry following the protocol as outlined by Reyes et al., (2002). Essentially, fixed cells were incubated in a blocking solution (5% goat serum in PBS) followed by an overnight incubation at 4°C with the primary antibody. Cells were then incubated with the appropriate secondary antibodies (1:200; Jackson), nuclei were stained with the fluorescent dye DAPI (4′,6-diamidino-2-phenylindole; Invitrogen), mounted onto slides with Aquamount (Lerner Laboratories), and fluorescent images were obtained using an Olympus spinning disc confocal microscope (Olympus, IX83-DSU). Quantitative analysis of the results was done counting the antigen-positive and DAPI-positive cells (total number of cells) in 20 randomly selected fields, which resulted in counts of >2,000 cells for each experimental condition. The primary antibodies used for immunocytochemistry were against: CC1 (1:300; Calbiochem), MBP (1:1000; Covance), MOG (1:200; Millipore), NG2 (1:400; Millipore), neurofilament M (1:250; Millipore), Olig1 (1:500; Millipore), Olig2 (1:500; Millipore), PDGFr (1:200; Millipore), phospho-histone H3 (1:500; Millipore) and PLP (1:200; Thermo Scientific).

Incorporation of bromo-deoxyuridine

Twenty-four hour pulses of 10μM bromo-deoxyuridine (BrdU) (BD Pharmingen) were applied at 24, 48 and 72h post siRNA transfection (Figure 5A). After each BrdU pulse, cells were fixed and immunostained in order to determine the number of positive cells. Cells were fixed in 4% paraformaldehyde in PBS. After treatment with 6N HCl and 1% Triton X-100 to denature nuclear DNA, the cells were incubated in 0.1M sodium borate (in PBS and 1% Triton X-100) for 10min. Immunocytochemistry was done using anti-BrdU antibody (1:1000; BD Pharmingen) and anti-NG2 (1:400; Millipore) with the corresponding fluorescent secondary antibodies. The percentage of BrdU positive cells was estimated on the basis of the total number of NG2 positive cells.

Cell cycle time analysis

To examine cell cycle time, primary cultures of GFP labeled OPCs were used (Mallon et al., 2002). These cultures were incubated in a stage top chamber with 5% CO2 at 37°C, which was placed on the stage of a spinning disc confocal inverted microscope (Olympus, IX83-DSU) equipped with a motorized stage and an atmosphere regulator. Fluorescent images were obtained at 6min intervals. Individual clones of mouse OPCs were followed for a period of 30h. In these time-lapse experiments, ~20 clones were analyzed per experimental condition. MetaMorph (Molecular Devices) was used in the analysis of video microscopic image sequences. The MetaMorph software allows an investigator to cycle back-and-forth through the movie files frame-by-frame (minute-by-minute), facilitating the accurate determination of event time. To quantitatively analyze the dynamics of cell division, 120 cytokinetic events were randomly selected from movies at different time points. Cell proliferation was assessed by calculating the average cell cycle time (time between birth

cytokinesis and division cytokinesis) in different OPC clones. Tracking of cells was performed by visual observation of image sequences as described above. Tracking was performed forwards and backwards in time from each identified cytokinesis event to maximize the number of lineally related cytokinetic events identified. Furthermore, the percentage of cycling OPCs during the first 12h of the time-lapse experiment was performed by visual observation.

Caspase-3 assay

NucView 488 Caspase-3 substrate, a cell membrane-permeable fluorogenic caspase substrate designed for detecting caspase-3 activity within live cells in real time, was used in accordance with the manufacturer's recommendations (Biotium Inc). Briefly, OPC primary cultures were incubated in medium containing NucView 488 Caspase-3 substrate (final concentration 5μM) in a stage top chamber with 5% CO2 at 37°C, which was placed on the stage of a spinning disc confocal inverted microscope (Olympus, IX83-DSU). Fluorescent field images were obtained with a specific GFP filter at 6min intervals for a total of 24 hours. MetaMorph software was used to assess apoptotic cell death by calculating the percentage of Caspase-3 positive cells in a total of five experiments on four random fields.

MTT assay

The MTT survival assay was performed as described by Mosmann (1983). The sterile solution of MTT (Molecular Probes) was added to all wells and the micro plate was incubated at 37°C for 45min. The reaction was stopped by addition of SDS and the product was quantified by spectrophotometry at 570nm.

Co-culture of cortical neurons and OPCs

Cortical neurons were prepared from the brains of 1- to 2-day-old mouse pups using established procedures (Echeverria et al., 2005) with minor modifications. Briefly, brains were removed aseptically and placed into DMEM/F12 (Invitrogen). After the brains were dissected, the blood vessels and meninges were carefully removed under a dissecting microscope. Brain cortices were isolated and dissociated by digestion with a solution of 0.05% trypsin (Sigma) containing DNase I (0.06%) in Neurobasal medium for 10min at 37°C. The digestion reaction was stopped with Neurobasal medium containing 10% fetal bovine serum (Omega Scientific) and triturated by repeated passages (20 times) through a 10ml pipette. The cell suspension was filtered through a sterile cell strainer (70μm; BD Biosciences) into a 50ml centrifuge tube. The cells were pelleted by centrifugation at 200g for 5min, and resuspended in Neurobasal medium plus 2% (v/v) B27 supplemented with 0.25mM GlutaMax I (Invitrogen), 0.25mM glutamine (Invitrogen), and 100μg/ml gentamicin (Omega Scientific). High-density cultures (5×10^5cells, ~2500 cells/mm^2) were plated onto 20mm^2 tissue culture wells coated with poly-D-lysine (Sigma). The neurons were kept at 37°C in 95% air 5% CO2 for 7 days in vitro and used for co-cultures. After 7 days in vitro, cortical neuron cultures consisted of neurons essentially free from non-neural cells. Co-cultures were prepared by the addition of OPCs to the cultures of cortical neurons at a density of 3×10^5 cells/ml. These cultures were maintained in DMEM/F12, 1% FBS for 7 and 14 days.

Cell morphology assessment

Oligodendroglial cell morphology was evaluated using the procedure described by Sperber and McMorris (2001) with slight modifications. Individual MBP-positive cells were scored according to their morphological complexity in four categories, based on the length and number of primary processes, whether the processes were radially distributed, the relative development of secondary and tertiary processes, and the overall size of the cell, including the process arbor.

RT-PCR

Total RNA was isolated using TRIZOL reagent (Invitrogen) according to the instructions of the manufacturer. RNA content was estimated by measuring the absorbance at 260nm and the purity was assessed by measuring the ratio of absorbance: 260/280nm. PCR primers for Cav1.2 (F-CAGCTCATGCCAACATGAAT, R-TGCTTCTTGGGTTTCCCATA) and for Cav1.3 (F-AATGGCACGGAATGTAGGAG, R-GACGAAAAATGAGCCAAGGA) were designed based on published sequences by Rosati et al., (2011) and Xu et al., (2007) respectively. First-strand cDNA was prepared from 1μg of total RNA using SuperScriptTM III RNase H-reverse transcriptase (Invitrogen) and 1μg of oligo(dT). The mRNA samples were denaturated at 65°C for 5min. Reverse transcription was performed at 50°C for 55min and was stopped by heating the samples at 85°C for 5min. The cDNA was amplified by PCR using the Cav1.2 and Cav1.3 isoform-specific primers listed above and PCR Platinum Supermix reagent (Invitrogen). PCR conditions were as follows: 94°C for 2min, 40 cycles of 94°C for 30s, 58°C for 30s followed by 68°C for 2min. After completion of the 40 cycles, samples were incubated at 72°C for 10min. A β-actin positive control was run alongside the experimental samples, as well as a negative control with no reverse transcriptase. The PCR products were visualized on an ethidium bromide-stained agarose gel and the bands digitized using a Gel Doc™ EZ System (BioRad).

Quantitative real-time PCR

Total RNA was extracted from primary cultures of pure oligodendroglial cells and co-cultures of OPCs with cortical neurons using TRIZOL Reagent (Invitrogen), following the manufacturer's protocol. Samples were further purified by treatment with TURBO DNA-free™ (Ambion), followed by a second extraction with phenol-chloroform. RNA was reverse transcribed using iScript cDNA Synthesis Kit (BioRad) then analyzed for various transcript expressions. qPCR was set up using iQ SYBR Green Supermix (BioRad) and performed in triplicate as previously described (Ghiani et al., 2006) on an iCycler MyiQ Real Time PCR machine (BioRad). Negative controls (samples in which reverse transcriptase was omitted) were amplified individually using the same primer sets to ensure the absence of genomic DNA contamination. PCR amplification resulted in the generation of single bands. Amplification specificity was assessed by melting curves and standard curves made from serial dilutions of control RNA and were used for quantification. Data were normalized to the internal control glyceraldehyde-3-phosphate dehydrogenase (GAPDH). Primers used for real-time PCR were designed based on published sequences by Mattan et al., (2010), Li et al., (2008) and Conrad et al., (2009) (see Table II for primer sequences).

Western blot analysis

Total protein was collected from primary cultures of pure oligodendroglial cells and co-cultures of OPCs with cortical neurons. The final protein pellet was homogenized in lysis buffer containing 50mM Tris-HCl, 0.25% (w/v) sodium deoxycholate, 150mM NaCl, 1mM EDTA, 1% (w/v) Triton X-100, 0.1% (w/v) SDS, 1mM sodium vanadate, 1mM AEBSF, 10ug/ml aprotinin, 10ug/ml leupeptin, 10ug/ml pepstatin, and 4uM sodium fluoride. Western blots were performed as previously described (Ghiani et al., 2010). Twenty-five to thirty-five micrograms of total protein was loaded onto a 4–20% Tris-glycine gel (Invitrogen). Protein bands were detected by chemiluminescence using the Amersham ECL kit (GE Healthcare) with horseradish peroxidase-conjugated secondary antibodies (Cell Signaling). Relative intensities of the protein bands were quantified by scanning densitometry using the NIH Image Software Image J. Equal protein loading was verified by Ponceau S solution (Sigma) reversible staining of the blots and each extract was also analyzed for relative protein levels of P84, GAPDH and β-actin. The primary antibodies used for Western blots were against: Cav1.2 (1:1000; Alomone), Cav1.3 (1:1000; Alomone), GAPDH (1:10000; Genetex), MBP (1:1000; Covance), NG2 (1:400; Millipore), P84 (1:6000; Genetex), PLP (1:1000, Thermo Scientific), Tuj1 (1:3000; Covance), CNPase (1:1000; Millipore), MOG (1:1000; Millipore) and β-actin (1:10000; Sigma).

Calcium imaging

Methods were similar to those described previously (Paez et al., 2007). Briefly, primary cultures of OPCs were washed in serum and phenol red-free DMEM containing a final concentration of 4μM Fura-2 (AM) (TefLabs) plus 0.08% Pluronic F127 (Molecular Probes) to load dye into the cells, incubated for 45 min at 37°C, 5% CO_2, then washed four times in DMEM and stored in DMEM for 10min before being imaged. Resting Ca^{++} levels were measured in serum-free HBSS containing 2mM Ca^{++} but no Mg^{++}. Other measurements were made in HBSS. Calcium influx and resting Ca^{++} levels were measured on individual cells, and the results were pooled from five separate experiments for each condition. The fluorescence of Fura-2 was excited alternatively at wavelengths of 340 and 380nm by means of a high-speed wavelength-switching device (Lambda DG4; Sutter Instruments). A spinning disc confocal inverted microscope (Olympus, IX83-DSU) equipped with a CCD camera (Hamamatsu ORCA-R2) measured the fluorescence. Image analysis software (MetaFluor, Molecular Devices) allowed for the selection of several “regions of interest” within the field from which measurements are taken. To minimize bleaching, the intensity of excitation light and sampling frequency was kept as low as possible. In these experiments, measurements were made once every 2s.

Statistical Analysis

Normal distributions were tested in each data set using Kolmogorov-Smirnov tests. For data with normal distributions, single between-group comparisons were made by the Student paired t-test, and multiple comparisons were investigated by one-way ANOVA followed by Bonferroni’s multiple comparison tests to detect pair-wise between-group differences. All statistical tests were performed in Graphpad Prism (Graphpad Software). A fixed value of

$p<0.05$ for one tailed tests was the criterion for reliable differences between groups. Data are presented as mean ± SEM unless otherwise noted.

RESULTS

The role of VOCCs on OPC differentiation

The role of VOCCs on OPC differentiation was analyzed in primary cultures of mouse OPCs subjected to different pharmacological treatments in order to activate or block voltage-gated Ca^{++} uptake. Calcium influx mediated by VOCCs was induced by depolarization via elevated external potassium (K^+). Increasing external K^+ to 20mM has been proven to be an effective way to fully activate OPC VOCCs by plasma membrane depolarization (Paez et al., 2007; 2010). The effects of blocking VOCC dependent Ca^{++} influx was studied with the specific L-type channel inhibitor verapamil. Using this in vitro system we followed the morphological differentiation of OPCs (processes formation and branching) and the expression of oligodendrocyte stage specific markers. Our data show that the morphological differentiation as well as the expression of mature oligodendrocyte markers was significantly inhibited in cells treated with verapamil (Figure 1B, C and D). In contrast, OPCs depolarized with high K^+ displayed a more complex morphology and showed a significant increase in the expression of mature markers such as MBP, MOG and CC1 (Figure 1B, C and D). Interestingly, the maturation of OPCs treated with high K^+ in the presence of verapamil was similar to that observed in verapamil treated cultures (Figure 1B, C and D), suggesting that plasma membrane depolarization have no effect on OPC development if L-type VOCCs are block by specific inhibitors.

In order to obtain a direct correlation between these channels and OPC differentiation we knocked down the expression of VOCCs in primary cultures of mouse OPCs. Since more than 90% of the Ca^{++} influx after plasma membrane depolarization in OPCs is mediated by L-type Ca^{++} channels (Paez et al., 2010), we used small interfering RNAs (siRNAs) for the Cav1 family of α1 subunits that conducts L-type Ca^{++} currents. The α1 subunit of the L-type Ca^{++} channel is encoded by Cav1-genes consisting of four different subtypes referred to as Cav1.1 (α1S), Cav1.2 (α1C), Cav1.3 (α1D), and Cav1.4 (α1F); only Cav1.2 and Cav1.3 are expressed in the brain (Hell et al., 1993), and we have found by RT-PCR and Western blot that both Cav1.2 and Cav1.3 are expressed in cultured OPCs (Figure 2C). Twenty-four hours after plating, OPCs were transiently transfected with a combination of three different validated siRNA duplexes specific for Cav1.2 and Cav1.3, the sole pore-forming subunits of the voltage-dependent L-type Ca^{++} channel in OPCs (Zhang et al., 2014). siRNAs were selected to target three distinct Cav1.2 and Cav1.3 mRNA regions to enhance silencing (Table I). A negative siRNA control was designed to minimize sequence homology to any known vertebrate transcript and with a similar GC content as our siRNAs and used for sequence independent effects in all the siRNA experiments performed. To determine the percentage of siRNA-transfected cells, OPCs were treated with fluorescein-labeled dsRNA oligomers. Twenty-four hours after transfection, we found that 100% of the NG2 and Olig2 positive cells displayed some degree of siRNA fluorescent signal (Figure 2B). The function of Cav1.2/1.3 siRNAs was validated using semi quantitative RT-PCR and western blotting. Figure 2C shows a representative RT-PCR and western blot demonstrating

that Cav1.2/1.3 siRNA decreased Cav1.2/1.3 mRNAs and proteins in OPCs 72h after transfection. Additionally, Figure 2D shows the effect of Cav1.2/1.3 siRNA on L-type Ca^{++} uptake in OPCs. Consistent with the RT-PCR and western blot data, Cav1.2 siRNA reduced L-type Ca^{++} influx by approximately 75% after plasma membrane depolarization, whereas Cav1.3 siRNA reduced Ca^{++} influx by ~20% (Figure 2D). These data suggest that Cav1.2 is the principal pore-forming subunit of the voltage-dependent L-type Ca^{++} channel in OPCs.

Previous reports have shown that gap junctions can mediate the spread of Ca^{++} waves between oligodendrocytes and that primary oligodendrocyte cultures, in the absence of astrocytes, display gap junction-mediated calcium signaling (Takeda et al., 1995). To test whether gap junctions play a role in OPCs calcium response after plasma membrane depolarization, we performed calcium imaging experiments in the presence of a broad-spectrum gap junction blocker, carbenoxolone (Davidson and Baumgarten, 1988). Under these conditions, the amplitude of the Ca^{++} response as well as the percentage of responding cells were similar to those found in control conditions (Figure 2E). Thus, these data suggest that gap junctions between oligodendrocytes are not involved in the propagation of Ca^{++} transients after high K^+ stimulation in our experimental culture system.

Using the in vitro system described in Figure 3A we have monitored the morphological differentiation of OPCs and the expression of oligodendrocyte stage specific markers after mitogen removal. Our data show that morphological differentiation as well as expression of mature oligodendrocyte markers was significantly inhibited in Cav1.2 deficient cells (Figure 3B–F). Under conditions where OPCs were allowed to differentiate for 48h, Cav1.2 siRNAs induced a decrease in the proportion of cells that expressed the mature markers MBP and CC1, and an increase in cells that retained immature oligodendrocyte markers such as PDGFr, Olig1 and NG2 (Figure 3B and C). In addition, real-time PCR experiments performed with total mRNA extracted from Cav1.2 transfected OPCs showed a significant reduction in mRNA levels of several myelin proteins including MAG, PLP, MBP, and ceramide-galactosyl transferase (CGT), a key enzyme involved in the generation and maintenance of the myelin sheath (Figure 3D). Similar results were obtained in western blot experiments (Figure 3F). In contrast, the maturation of Cav1.3 knockdown OPCs as well as their expression level of myelin proteins was similar to that observed in control cells (Figure 3B–F). OPC morphology was evaluated using the procedure described by Sperber and McMorris (2001). Seventy-two hours after siRNAs transfection, individual MBP-positive OPCs were scored according to their morphological complexity in four different categories. In control cultures, the percentage of cells of low and medium complexity was 54% and 36% respectively, while the percentage of cells with medium-high complexity was 12% (Figure 3E). After 72h of Cav1.2 siRNAs transfection, the percentage of cells with low complexity increased markedly (68%), while there was a significant decrease in the percentage of cells with medium (25%) and medium-high morphology (5%) (Figure 3E). In agreement with the immunocytochemistry results, the morphological differentiation of Cav1.3 knockdown OPCs was similar to that observed in control cells (Figure 3E). Furthermore, 24h after siRNAs transfection, OPCs were treated with high K^+ in order to activate voltage-gated Ca^{++} uptake in Cav1.2 knockdown cells. Two days after high K^+ treatment we found no changes in the maturation of Cav1.2 knockdown OPCs compare to non-stimulated transfected cells (Figure 3C), suggesting that Ca^{++} influx mediated by

Cav1.2 channels is essential for the effect of plasma membrane depolarization on OPC development.

In order to explore the role of VOCCs in the development of premyelinating oligodendrocytes, cells were transfected with Cav1.2/1.3 siRNAs after two days of mitogen deprivation (Figure 4A). We have found that after shifting to the differentiation medium (mN2) there is a sharp increase in mature (e.g. CC1, MBP) markers consistent with differentiation of the OPCs (Paez et al., 2009b). Suggesting a role for VOCCs during the first steps of OPC development, our data show that the morphological differentiation and the expression of mature oligodendrocyte markers were not affected in newly generated oligodendrocytes after 72h of being treated with siRNAs for L-type VOCCs (Figure 4B–D).

The function of L-type VOCCs on the proliferation and survival of OPCs

We have performed experiments to assess the effect of knocking down the expression of L-type VOCCs on OPC proliferation. Since actively proliferating cells duplicate their DNA content, we labeled proliferating OPCs from control and siRNA-transfected cultures with the thymidine analogue bromo-deoxyuridine (BrdU) over a period of three days. Twenty-four hours pulses of 10μM BrdU were given at 24h, 48h and 72h after transfection (Figure 5A). After each BrdU pulse, proliferating progenitors were identified by double immunofluorescence for BrdU and NG2 and the relative number of $BrdU^+/NG2^+$ cells was quantified in each cell population (Figure 5B and D). We found that OPC proliferation was lower in the Cav1.2 transfected populations than control cultures (Figure 5B and D). For example, after 48h the average number of proliferating cells in the Cav1.2 transfected cultures (12%) was significantly lower than that of the control group (23%, $P<0.01$) (Figure 5D). Similar results were found at 24 and 72 hours after transfection (Figure 5D). Since growth factors played an essential role in OPCs division, parallel experiments were done to assess the proliferation of siRNA transfected OPCs in the presence of PDGF. OPCs were transfected with siRNA duplexes specific for Cav1.2/1.3 and cultured during three days in defined culture media (Agresti et al., 1996) containing PDGF (10ug/ml). Under these experimental conditions and in agreement with our previous results after growth factors withdrawal, OPCs lacking Cav1.2 showed decreased levels of proliferation compare to control cells (Figure 5D). Confirmation of the BrdU cell proliferation results was performed using an anti Phospho-Histone-H3 antibody as a marker of mitotic cells (Wei et al., 1999). In agreement with our previous findings, Cav1.2 knockdown was able to significantly decrease the total number of Phospho-Histone $H3^+$ OPCs at all the time points evaluated (Figure 5C and E). Moreover, no significant differences were found in the proliferation rate of Cav1.3 transfected OPCs versus control cells (Figure 5D and E).

Next, we measured the cell cycle times of Cav1.2/1.3 transfected OPCs by performing time-lapse imaging in primary cultures. The OPCs used in these experiments were isolated from transgenic mice expressing GFP under control of the PLP promoter (Mallon et al., 2002). In these mice, GFP expression provides a convenient marker for OPCs in time-lapse experiments. We imaged individual clones of GFP-labeled OPCs for a period of 30h. In these time-lapse experiments, cell proliferation was assessed by calculating the average cell cycle time in different OPC clones. Cell cycle time was defined as the period between when

a cell was first generated by cytokinesis and when that cell subsequently divided, giving two daughter cells (Paez et al., 2009b). Examples of cytokinetic events in GFP-labeled control OPCs tracked for 24h are shown in Figure 6A. One hundred twenty cytokinetic events were randomly selected from movies at different time points. Tracking of cells was performed by visual observation of image sequences as described previously (Paez et al., 2009b). Control OPCs showed a cell cycle time of ~23h, whereas the cell cycle time of OPCs transfected with Cav1.2 siRNAs was increased to ~28h and ~27h after 48h and 72h of siRNA transfection respectively (Figure 6B). Similar experiments were performed in the presence of PDGF. Although there was an increase in the cell replication speed of control OPCs in the presence of PDGF, the cell cycle time of Cav1.2 deficient cells was similar to what we found after growth factors withdrawal (Figure 6B). Furthermore, as shown in Figure 6C, the percentage of cycling OPCs during the first 12h of the time-lapse experiment was lower in the Cav1.2 transfected cultures suggesting that the fraction of proliferating OPCs is decreased after L-type VOCC knockdown. These results indicate by several independent measures that Cav1.2 knockdown diminished OPC proliferation, i.e. decreased the number of mitotic cells and increased the duration of the cell cycle. Additionally, Cav1.3 transfected OPCs showed no significant changes in cell division relative to control (Figure 6B and C), suggesting that this particular L-type α1 subunit is not involved in modulating OPC proliferation.

The consequence of L-type VOCCs knockdown on OPC survival was examined using the MTT quantitative colorimetric method for cell viability. The results revealed no significant differences between groups 48h after siRNA transfection (Figure 7C). Cav1.2 siRNA transfected OPCs showed no changes in cell viability relative to control (Figure 7C), suggesting that the decrease in cell maturation and proliferation found in these cultures are not a consequence of cell death. We also examined the role of L-type VOCC on OPC apoptotic cell death in Cav1.2/1.3 deficient OPCs. We used a real-time Caspase-3 assay, which detects caspase-3 activation within individual living cells. This assay is bi-functional in that it is able to detect both intracellular caspase-3 activity and also stain the cell nucleus, which undergoes morphological changes during the apoptotic process (Paez et al., 2009b). Examples of such measurements in Cav1.2 transfected OPCs are shown in Figure 7A. Consistent with the MTT results, the combined use of real time confocal microscopy and the caspase-3 indicator revealed that OPCs transfected with siRNAs for Cav1.2/1.3 showed no increase in the percentage of apoptotic cells relative to controls (Figure 7B).

The role of VOCCs on oligodendrocyte-neuron interaction

In this group of experiments we used a co-culture system of OPCs with cortical neurons to analyze the role of L-type VOCCs on the early phases of myelination. Twenty-four hours after siRNA transfection, OPCs were added to cortical neuron cultures prepared from the brains of mouse pups (Echeverria et al., 2005). Using this in vitro model of myelination, we analyzed the interaction of OPCs with neurites and the elaboration of myelin membrane structures by these cells as described previously (Paez et al., 2005). Initially, GFP-labeled OPCs (Mallon et al., 2002) were co-cultured with cortical neurons for 7 days and the number of contacts with neurites, including the elaboration of myelin membrane structures, was analyzed by confocal microscopy. As show in Figure 8A there was a noticeable change

in the morphology of control OPCs, from rounded cells with few processes to a highly branching, reticulated structures. Many cell extensions seemed to be in close contact with neurites (Figure 8A). Although in Cav1.2 transfected cells, there was a change in cell morphology when co-cultured with cortical neurons, processes formation and elaboration of membranous sheets were much less extensive than in the control cells (Figure 8B). Analysis of the morphological complexity according to Sperber and McMorris (2001) showed that knocking down the expression of Cav1.2 markedly decreased the percentage of cells with medium, medium-high and high complexity, and increased the percentage of cells with low complexity (Figure 8C). Furthermore, the average number of contact points with neurites was significantly reduced when the co-culture included Cav1.2 transfected OPCs (Figure 8D). To establish whether siRNA treated OPCs were able to myelinate axons, we evaluated the expression of oligodendrocyte differentiation markers and myelin related proteins by immunocytochemistry, real-time PCR and western blot. Figure 9 shows examples of NG2 and PLP positive cells after 7 days of co-culture. In the control group nearly all the NG2 expressing cells as well as the PLP positive oligodendrocytes were interacting with neurons (Figure 9A and C). Although we found a small proportion of NG2 transfected cells interacting with neurons, none of the PLP positive Cav1.2 transfected cells established contact with cortical neurons (Figure 9B and D). Similarly, control cells expressing MBP interact extensively with cortical neurons and show complex morphology, whereas Cav1.2 transfected cells display a much simpler morphology and nearly no contact points with neurons (Figure 10A and B). Real-time PCR experiments performed with total mRNA extracted from co-cultures of Cav1.2 deficient cells showed a significant reduction in mRNA levels of myelin proteins (Figure 10C). In the same line, we found a significant decline in the expression of MBP, MOG, PLP and CNPase and a substantial rise in NG2 expression by western blot in Cav1.2 deficient co-cultures (Figure 10E). Furthermore, OPC maturation was analyzed in co-cultures at 14 days in vitro. Figure 11A and B show examples of NG2 and MBP positive cells grew for 14 days in the presence of neurons. Compared with 7 days old co-cultures, control cells displayed a more complex morphology, higher levels of myelin proteins expression and more contact points with neurons (Figure 11A–E). On the contrary, two weeks of co-culture did not significantly improve the maturation of OPCs lacking L-type VOCCs, which showed low percentage of cells expressing MBP and PLP and few contact points with neurons (Figure 11A–E). In agreement with our previous experiments in primary cultures of OPCs, high K^+ treatment increases the number and the morphological maturation of control MBP positive cells but do not promotes the maturation of Cav1.2 knockdown OPCs in co-culture (Figure 11F–H). These data suggest that depolarization of neurons and OPCs in co-culture stimulate the maturation of only L-type VOCC expressing OPCs. In summary, this set of in vitro experiments established a key role for the L-type VOCC subunit Cav1.2 in the development and differentiation of OPCs and in the early phases of the oligodendrocyte-neuron interaction.

DISCUSSION

L-type VOCCs are essential for OPC maturation

L-type calcium channels are essential for the normal development of neuronal progenitors playing established roles in regulating gene expression, cell survival and synaptic plasticity (Gallin and Greenberg, 1995; Mao et al. 1999; Marshall et al. 2003; Murphy et al. 1991; Norris et al. 1998; Weisskopf et al. 1999; Yagami et al, 2012). We hypothesized that L-type VOCCs are also important for OPC development, probably by the activation of similar Ca^{++}-dependent intracellular pathways. Clearly indicating that VOCCs are essential for OPC maturation, the morphological differentiation as well as the expression of mature oligodendrocyte markers was significantly repressed in cells treated with specific VOCC inhibitors. In contrast, OPCs treated with high K^+ displayed a more complex morphology and showed a significant increase in the expression of mature markers. In the same line, blocking the expression of the α1.2 subunit that conducts L-type Ca^{++} currents significantly prevents OPC processes extension, morphological maturation and as a consequence, myelin proteins expression. The effect of knocking down the expression of Cav1.2 on OPC differentiation could be interpreted either as inhibition or delay of the normal maturational process. However, since the effect of knocking down Cav1.2 on OPC differentiation persisted three days after growth factor withdrawal in a pro-differentiation culture media, we believe that the absence of L-type VOCCs is inhibiting OPC maturation.

We have found that the two main α1 subunits of the L-type Ca^{++} channel present in the brain are expressed in OPCs. Using calcium imaging analysis and specific siRNAs we have shown that over 75% of the Ca^{++} uptake after plasma membrane depolarization is mediated by Cav1.2 containing channels and less than 20% is associated with Cav1.3 expressing VOCCs. Suggesting that Cav1.3 is not involve in modulating oligodendrocyte development, Cav1.3 deficient OPCs show normal expression of myelin proteins, regular morphological maturation and no significant differences in the proliferation rate versus control cells. These data suggest that Cav1.2 is the principal pore-forming subunit of the voltage-dependent L-type Ca^{++} channel in OPCs and unlike Cav1.3, is essential for proper OPC maturation.

OPCs from the mouse cortex (Verkhratsky et al., 1990; von Blankenfeld et al., 1992) exhibit both low voltage-activate (LVA) and high-voltage activated (HVA) Ca^{++} currents (Williamson et al., 1997). Recordings from early postnatal slices revealed the presence of both HVA and LVA Ca^{++} currents in OPCs located in white matter regions (Berger et al., 1992; Fulton et al., 2010). Several studies have reported that Ca^{++} responses through VOCCs appear to diminish with maturation of oligodendrocytes from progenitors to mature cells in culture (Berger et al., 1992; Takeda et al., 1995). We have previously shown that OPCs responded to depolarization with large increases in intracellular Ca^{++} whereas more mature oligodendrocytes responded with a significantly smaller increase in the Fura-2 signal under the same high K^+ treatment (Paez et al., 2010). Additionally, voltage-operated Ca^{++} influx was significantly greater in OPCs from the sub-ventricular zone compared to more mature oligodendrocytes found in the corpus callosum (Paez et al., 2010). A recently published RNA-sequencing transcriptome database of glial, neurons, and vascular cells of the cerebral cortex, reveal high expression of L-type Ca^{++} channel subunits in OPCs and

downregulation of L-type VOCCs in newly formed and myelinating oligodendrocytes (Zhang et al., 2014). The in vitro and in situ data reveal that voltage-operated Ca^{++} influx present in OPCs and immature oligodendrocytes disappear as the cells matured. It is likely that voltage-operated Ca^{++} influx plays a role during the first steps of OPC maturation because expression of VOCCs decreases during development. In this work we have established that the development of newly generated oligodendrocytes, unlike OPCs was not affected by the L-type Ca^{++} channel knockdown indicating that there is a precise and narrow time window in which VOCCs affect OPC maturation and myelination.

L-type Ca^{++} channels modulate OPC proliferation

L-type calcium channels play a key role in the proliferation and differentiation of non-excitable cells such as bone marrow mesenchymal stem cells and T-lymphocytes (Wen et al., 2012; Kotturi et al., 2003). Blocking L-type VOCC significantly inhibited bone marrow mesenchymal stem cell proliferation and the osteogenic differentiation of this cells in vitro (Wen et al., 2012). Furthermore, L-type Ca^{++} uptake is required for T-lymphocyte activation and proliferation during an immune response (Kotturi et al., 2003). Our data reveal that Cav1.2 knockdown decreased OPC proliferation, as the proportion of NG2 positive OPCs that incorporated BrdU significantly decreased compared with control cells. Cav1.2 deficient OPCs proliferated less robustly and showed a significant increase in the length of the cell cycle after growth factor withdrawal. The differences we noted in cell proliferation are likely explained by changes in the cell cycle duration, since the length of the cell cycle time could progressively increase the probability that an OPC stops dividing (Gao et al., 1998; Tang et al., 2000). Interestingly, the mitotic activity of OPCs lacking Cav1.2 was also diminished in the presence of PDGF. PDGF is the best characterized and the most active proliferative factor for OPCs. It exerts its effect through interaction with receptors bearing intrinsic tyrosine kinase activity (Taniguchi, 1995). Ca^{++} signals activated after membrane receptor recruitment is one of the most conserved responses triggered in the target cells in which PDGF exert a mitogenic activity (Fatatis and Miller, 1997). In a previous work we have shown that store-operated Ca^{++} entry as well as Ca^{++} release from intracellular stores are essential components of the PDGF mitotic mechanism in OPCs (Paez et al., 2009b). Our present data suggest that the absence of Cav1.2 disrupt OPC response to PDGF and more importantly that Ca^{++} influx mediated by L-type VOCCs is critical for the effect of this growth factor on the cell cycle. Our current hypothesis is that Ca^{++} uptake mediated by L-type channels modulates OPC division and maturation through independent intracellular pathways. VOCCs seem to be essential for the normal progression of the cell cycle in mitotic OPCs, but after cell cycle exit, the same channels are playing an important role in the maturation of oligodendrocytes.

L-type Ca^{++} channels seems to be required in the communication between oligodendrocytes and neurons

A potential mechanism for axon-glial signaling involves axonal activity-induced accumulation of extracellular K^+ sufficient to depolarize L-type VOCCs in nearby glial cells. Kirischuk and co-workers (1995) showed that physiological range increases in extracellular K^+ are sufficient to produce a significant rise in intracellular Ca^{++} in OPCs, and that K^+ concentrations higher than physiological were found close to active axons

during myelination. ATP and glutamate are also released from axons during electrical impulse activity (Agresti et al., 2005; Kirchhoff and Kettenmann, 1992; Kastritsis and McCarthy, 1993; Patneau et al., 1994). ATP and glutamate receptor-mediated Ca^{++} signaling in OPCs is initiated by an increased influx of Na^{+} and Ca^{++} through the activated receptor. Subsequently Na^{+} influx can depolarize the OPC plasma membrane making neuronal ATP and glutamate an alternative way to stimulate OPC L-type VOCCs. Chen et al. (2000) found strong, transient expression of VOCCs in CNS white matter. VOCC immunoreactivity was located in oligodendroglial somata, projections, paranodal wraps and loose myelin sheaths. We hypothesize that OPC projections contacting axons sense axonal firing via the depolarization of OPC VOCCs caused by the elevations in external K^{+}, ATP and glutamate that follow neuronal firing. This VOCC activation may in turn stimulate the Ca^{++} signals that lead to myelination. It is thus plausible that the detection of axonal activity through changes in extracellular [K^{+}], [ATP] and [glutamate] by VOCCs facilitate axon-glial signaling during the initial stages of myelin formation. In this paper, we showed that Cav1.2 deficient OPCs were less effective in establishing contacts with neurites and axons in co-culture with cortical neurons. The morphological differentiation and the expression of myelin proteins by these cells were drastically repressed even in the presence of neurons. These data suggest that OPC-expressed L-type Ca^{++} channels play a specific role in myelination during development. Loss of Cav1.2 in OPCs affects axonal contact and consequently the initial steps of myelination. Furthermore, it is likely that factors involved in normal myelination participate in remyelination of the injured CNS. Calcium channels implicated in OPC differentiation and maturation may induce positive signals for recovery. In this regard, a significant increase in the activity of OPC L-type VOCCs was found in the demyelinated corpus callosum of mice treated with cuprizone (Paez et al., 2012), suggesting that these channels may play a fundamental role in the induction and/or survival of newly generated OPCs during a demyelination event.

An important mode of communication between various cell types in the central nervous system involves gap junctions. Contrary to Takeda et al. (1995) we did not find gap junction-mediated Ca^{++} signaling in our primary OPC cultures. However, the presence of gap junctions between oligodendrocytes and astrocytes has been well documented in vitro as well as in vivo (Takeda et al., 1995; Rash et al., 2001). Evidence for gap junction-mediated Ca^{++} transfer between these two glial cell populations was recently reported (Parys et al., 2010). Parys and collaborators showed that waves of Ca^{++} spread from astrocytes to oligodendrocytes in a bi-directional fashion and that these waves are inhibited by specific gap junction blockers (Parys et al., 2010). Therefore, VOCC activation in OPCs triggered by surrounding neuronal activity might be able to feed back onto different neuronal and oligodendroglial populations through astrocytes. This gap junction mediated intercellular Ca^{++} signaling via oligodendrocyte-astrocyte-neuron pathway may represent a new mechanism of interaction between glial cells and neurons in the central nervous system.

In summary, we demonstrated that selective deletion of Cav1.2 in oligodendroglia exerts profound effects on OPC development. L-type Ca^{++} channels drive important effects that influence OPC proliferation and maturation, specifically the initial stages of myelination. We tested new hypotheses related to understanding the molecular events governing OPC

development and we have provided clues into molecular events that may be manipulated to encourage remyelination after demyelinating episodes in the brain.

Acknowledgments

Grant sponsors: NIH/NINDS grant 1R01NS078041-01A1 and National Multiple Sclerosis Society Grant RG4554-A-2.

REFERENCES

Agresti C, Meomartini ME, Amadio S, Ambrosini E, Volonté C, Aloisi F, Visentin S. ATP regulates oligodendrocyte progenitor migration, proliferation, and differentiation: involvement of metabotropic P2 receptors. Brain Res Rev. 2005; 48:157–165. [PubMed: 15850654]

Agresti C, D'Urso D, Levi G. Reversible inhibitory effects of interferon-γ and tumour necrosis factor-α on oligodendroglial lineage cell proliferation and differentiation in vitro. Eur J Neurosci. 1996; 8:1106–1116. [PubMed: 8752580]

Alberdi E, Sanchez-Gomez MV, Matute C. Calcium and glial cell death. Cell Calcium. 2005; 38:417–425. [PubMed: 16095689]

Amur-Umarjee S, Phan T, Campagnoni AT. Myelin basic protein mRNA translocation in oligodendrocytes is inhibited by astrocytes in vitro. J Neurosci Res. 1993; 36:99–110. [PubMed: 7693963]

Belachew S, Malgrange B, Rigo JM, Rogister B, Leprince P, Hans G, Nguyen L, Moonen G. Glycine triggers an intracellular calcium influx in oligodendrocyte progenitor cells which is mediated by the activation of both the ionotropic glycine receptor and Na^+-dependent transporters. Eur J Neurosci. 2000; 12:1924–1930. [PubMed: 10886333]

Benjamins JA, Nedelkoska L. Release of intracellular calcium stores leads to retraction of membrane sheets and cell death in mature mouse oligodendrocytes. Neurochem Res. 1996; 21:471–479. [PubMed: 8734441]

Berger T, Schnitzer J, Orkand PM, Kettenmann H. Sodium and calcium currents in glial cells of the mouse corpus callosum slice. Eur J Neurosci. 1992; 4:1271–1284. [PubMed: 12106391]

Chen S, Ren YQ, Bing R, Hillman DE. Alpha 1E subunit of the R-type calcium channel is associated with myelinogenesis. J Neurocytol. 2000; 29:719–728. [PubMed: 11387546]

Conrad AH, Albrecht M, Pettit-Scott M, Conrad GW. Embryonic corneal Schwann cells express some Schwann cell marker mRNAs, but no mature Schwann cell marker proteins. Invest Ophthalmol Vis Sci. 2009; 50:4173–4184. [PubMed: 19387082]

Davidson JS, Baumgarten IM. Glycyrrhetinic acid derivatives: a novel class of inhibitors of gap-junctional intercellular communication. Structure-activity relationships. J Pharmacol Exp Ther. 1988; 246:1104–1107. [PubMed: 3418512]

Deitmer JW, Verkhratsky AJ, Lohr C. Calcium signaling in glial cells. Cell Calcium. 1998; 24:405–416. [PubMed: 10091009]

Echeverria V, Greenberg D, Dore S. Expression of Prostaglandin E_2 Synthases in Mouse Postnatal Cortical Neurons. Ann NY Acad Sci. 2005; 1053:460–471. [PubMed: 16179554]

Fatatis A, Miller RJ. Platelet-derived growth factor (PDGF)-induced Ca^{++} signaling in the CG4 oligodendroglial cell line and in transformed oligodendrocytes expressing the PDGF receptor. J Biol Chem. 1997; 272:4351–4358. [PubMed: 9020156]

Fulton D, Paez PM, Fisher R, Handley V, Colwell CS, Campagnoni AT. Regulation of L-type Ca^{++} currents and process mophology in white matter oligodendrocyte precursor cells by golli-myelin proteins. Glia. 2010; 58:1292–1303. [PubMed: 20607717]

Gallin WJ, Greenberg ME. Calcium regulation of gene expression in neurons: the mode of entry matters. Curr Opin Neurobiol. 1995; 5:367–374. [PubMed: 7580160]

Gao FB, Apperly J, Raff M. Cell-intrinsic timers and thyroid hormone regulate the probability of cell-cycle withdrawal and differentiation of oligodendrocyte precursor cells. Dev Biol. 1998; 197:54–66. [PubMed: 9578618]

Ghiani CA, Lelievre V, Beltran-Parrazal L, Sforza DM, Malvar J, Smith DJ, Charles AC, Ferchmin PA, de Vellis J. Gene expression is differentially regulated by neurotransmitters in embryonic neuronal cortical culture. J Neurochem. 2006; 97:35–43. [PubMed: 16635248]

Ghiani CA, Starcevic M, Rodriguez-Fernandez IA, Nazarian R, Cheli VT, Chan LN, Malvar JS, de Vellis J, Sabatti C, Dell'Angelica EC. The dysbindin-containing complex (BLOC-1) in brain: developmental regulation, interaction with SNARE proteins and role in neurite outgrowth. Mol Psychiatry. 2010; 15:204–215.

Hell JW, Westenbroek RE, Warner C, Ahlijanian MK, Prystay W, Gilbert MM, Snutch TP, Catterall WA. Identification and differential subcellular localization of the neuronal class C and class D L-type calcium channel alpha 1 subunits. J Cell Biol. 1993; 123:949–962. [PubMed: 8227151]

Kastritsis CH, McCarthy KD. Oligodendroglial lineage cells express neuroligand receptors. Glia. 1993; 8:106–113. [PubMed: 8104891]

Kirchhoff F, Kettenmann H. GABA triggers a [Ca^{2+}]i increase in murine precursor cells of the oligodendrocyte lineage. Eur J Neurosci. 1992; 4:1049–1058. [PubMed: 12106410]

Kirischuk S, Scherer J, Moller T, Verkhratsky A, Kettenmann H. Subcellular heterogeneity of voltage-gated Ca^{2+} channels in cells of the oligodendrocyte lineage. Glia. 1995; 13:1–12. [PubMed: 7751051]

Kotturi MF, Carlow DA, Lee JC, Ziltener HJ, Jefferies WA. Identification and functional characterization of voltage-dependent calcium channels in T lymphocytes. J Biol Chem. 2003; 278:46949–46960. [PubMed: 12954628]

Li J, Ghiani CA, Kim JY, Liu A, Sandoval J, DeVellis J, Casaccia-Bonnefil P. Inhibition of p53 transcriptional activity: a potential target for future development of therapeutic strategies for primary demyelination. J Neurosci. 2008; 28:6118–6127. [PubMed: 18550754]

Mallon BS, Shick HE, Kidd GJ, Macklin WB. Proteolipid promoter activity distinguishes two populations of NG2-positive cells throughout neonatal cortical development. J Neurosci. 2002; 22:876–885. [PubMed: 11826117]

Mao Z, Bonni A, Xia F, Nadal-Vicens M, Greenberg ME. Neuronal activity-dependent cell survival mediated by transcription factor MEF2. Science. 1999; 286:785–790. [PubMed: 10531066]

Marshall J, Dolan BM, Garcia EP, Sathe S, Tang X, Mao Z, Blair LA. Calcium channel and NMDA receptor activities differentially regulate nuclear C/EBPbeta levels to control neuronal survival. Neuron. 2003; 39:625–639. [PubMed: 12925277]

Mattan NS, Ghiani CA, Lloyd M, Matalon R, Bok D, Casaccia P, de Vellis J. Aspartoacylase deficiency affects early postnatal development of oligodendrocytes and myelination. Neurobiol Dis. 2010; 40:432–443. [PubMed: 20637282]

Mosmann T. Rapid colorimetric assay for cellular growth and survival: application to proliferation and cytotoxicity assays. J. Immunol Methods. 1983; 65:55–63. [PubMed: 6606682]

Murphy TH, Worley PF, Baraban JM. L-type voltage-sensitive calcium channels mediate synaptic activation of immediate early genes. Neuron. 1991; 7:625–635. [PubMed: 1657056]

Norris CM, Halpain S, Foster TC. Reversal of age-related alterations in synaptic plasticity by blockade of L-type Ca2+ channels. J Neurosci. 1998; 18:3171–3179. [PubMed: 9547225]

Oh LY, Denninger A, Colvin JS, Vyas A, Tole S, Ornitz DM, Bansal R. Fibroblast growth factor receptor 3 signaling regulates the onset of oligodendrocyte terminal differentiation. J Neurosci. 2003; 23:883–894. [PubMed: 12574417]

Paez PM, García CI, Campagnoni AT, Soto EF, Pasquini JM. Overexpression of human transferrin in two oligodendroglial cell lines enhances their differentiation. Glia. 2005; 52:1–15. [PubMed: 15892129]

Paez PM, Spreuer V, Handley V, Feng JM, Campagnoni C, Campagnoni AT. Increased expression of golli myelin basic proteins enhances calcium influx into oligodendroglial cells. J Neurosci. 2007; 27:12690–12699. [PubMed: 18003849]

Paez PM, Fulton DJ, Spreuer V, Handley V, Campagnoni CW, Macklin WB, Colwell C, Campagnoni AT. Golli myelin basic proteins regulate oligodendroglial progenitor cell migration through voltage-gated Ca^{++} influx. J Neurosci. 2009a; 29:6663–6676. [PubMed: 19458236]

Paez PM, Fulton DJ, Spreuer V, Handley V, Campagnoni CW, Campagnoni AT. Regulation of store-operated and voltage-operated Ca^{++} channels in the proliferation and death of oligodendrocyte precursor cells by Golli proteins. ASN-Neuro. 2009b; 1:25–41.

Paez PM, Fulton DJ, Spreur V, Handley V, Campagnoni AT. Multiple kinase pathways regulate voltage-dependent Ca^{++} influx and migration in oligodendrocyte precursor cells. J Neurosci. 2010; 30:6422–6433. [PubMed: 20445068]

Paez PM, Cheli VT, Spreuer V, Handley V, Campagnoni AT. Golli myelin basic proteins stimulate oligodendrocyte progenitor cell proliferation and differentiation in remyelinating adult mouse brain. Glia. 2012; 60:1078–1093. [PubMed: 22447683]

Parys B, Côté A, Gallo V, De Koninck P, Sík A. Intercellular calcium signaling between astrocytes and oligodendrocytes via gap junctions in culture. Neuroscience. 2010; 167:1032–1043. [PubMed: 20211698]

Patneau DK, Wright PW, Winters C, Mayer ML, Gallo V. Glial cells of the oligodendrocyte lineage express both kainate- and AMPA preferring subtypes of glutamate receptor. Neuron. 1994; 12:357–371. [PubMed: 7509160]

Rash JE, Yasumura T, Davidson KGV, Furman CS, Dudek FE, Nagy JI. Identification of Cells Expressing Cx43, Cx30, Cx26, Cx32 and Cx36 in Gap Junctions of Rat Brain and Spinal Cord. Cell Commun Adhes. 2001; 8:315–320. [PubMed: 12064610]

Reyes SD, Campagnoni AT. Two separate domains in the golli myelin basic proteins are responsible for nuclear targeting and process extension in transfected cells. J Neurosci Res. 2002; 69:587–596. [PubMed: 12210824]

Rosati B, Yan Q, Lee MS, Liou SR, Ingalls B, Foell J, Kamp TJ, McKinnon D. Robust L-type calcium current expression following heterozygous knockout of the Cav1.2 gene in adult mouse heart. J Physiol. 2011; 589:3275–3288. [PubMed: 21521762]

Simpson PB, Armstrong RC. Intracellular signals and cytoskeletal elements involved in oligodendrocyte progenitor migration. Glia. 1999; 26:22–35. [PubMed: 10088669]

Simpson PB, Mehotra S, Lange GD, Russell JT. High density distribution of endoplasmic reticulum proteins and mitochondria at specialized Ca^{2+} release sites in oligodendrocyte processes. J Biol Chem. 1997; 272:22654–22661. [PubMed: 9278423]

Soliven B. Calcium signalling in cells of oligodendroglial lineage. Microsc Res Tech. 2001; 52:672–679. [PubMed: 11276119]

Sperber BR, McMorris FA. Fyn tyrosine kinase regulates oligodendroglial cell development but is not required for morphological differentiation of oligodendrocytes. J Neurosci Res. 2001; 63:303–312. [PubMed: 11170180]

Suzumura A, Bhat S, Eccleston PA, Lisak RP, Silberberg DH. The isolation and long-term culture of oligodendrocytes from newborn mouse brain. Brain Res. 1984; 324:379–383. [PubMed: 6397235]

Takeda M, Nelson DJ, Soliven B. Calcium signaling in cultured rat oligodendrocytes. Glia. 1995; 14:225–236. [PubMed: 7591034]

Tang DG, Tokumoto YM, Raff MC. Long-term culture of purified postnatal oligodendrocyte precursor cells: evidence for an intrinsic maturation program that plays out over months. J Cell Biol. 2000; 148:971–984. [PubMed: 10704447]

Taniguchi T. Cytokine signaling through nonreceptor protein tyrosine kinases. Science. 1995; 268:251–255. [PubMed: 7716517]

Verkhratsky AN, Trotter J, Kettenmann H. Cultured glial precursor cells from mouse cortex express two types of calcium currents. Neurosci Lett. 1990; 112:194–198. [PubMed: 2163037]

von Blankenfeld G, Verkhratsky AN, Kettenmann H. Ca^{2+} channel expression in the oligodendrocyte lineage. Eur J Neurosci. 1992; 4:1035–1048. [PubMed: 12106409]

Weisskopf MG, Bauer EP, LeDoux JE. L-type voltage-gated calcium channels mediate NMDA-independent associative long-term potentiation at thalamic input synapses to the amygdala. J Neurosci. 1999; 19:10512–10519. [PubMed: 10575047]

Wei Y, Yu L, Bowen J, Gorovsky MA, Allis CD. Phosphorylation of histone H3 is required for proper chromosome condensation and segregation. Cell. 1999; 97:99–109. [PubMed: 10199406]

Wen L, Wang Y, Wang H, Kong L, Zhang L, Chen X, Ding Y. L-type calcium channels play a crucial role in the proliferation and osteogenic differentiation of bone marrow mesenchymal stem cells. Biochem Biophys Res Commun. 2012; 424:439–445. [PubMed: 22771798]

Williamson AV, Compston DA, Randall AD. Analysis of the ion channel complement of the rat oligodendrocyte progenitor in a commonly studied in vitro preparation. Eur J Neurosci. 1997; 9:706–720. [PubMed: 9153577]

Xu JH, Long L, Tang YC, Hu HT, Tang FR. Ca(v)1.2, Ca(v)1.3, and Ca(v)2.1 in the mouse hippocampus during and after pilocarpine-induced status epilepticus. Hippocampus. 2007; 17:235–251. [PubMed: 17265461]

Yagami T, Kohma H, Yamamoto Y. L-type voltage-dependent calcium channels as therapeutic targets for neurodegenerative diseases. Curr Med Chem. 2012; 19:4816–4827. [PubMed: 22834820]

Yoo AS, Krieger C, Kim SU. Process extension and intracellular Ca^{2+} in cultured murine oligodendrocytes. Brain Res. 1999; 827:19–27. [PubMed: 10320689]

Zhang Y, Chen K, Sloan SA, Bennett ML, Scholze AR, O'Keeffe S, Phatnani HP, Guarnieri P, Caneda C, Ruderisch N, Deng S, Liddelow SA, Zhang C, Daneman R, Maniatis T, Barres BA, Wu JQ. An RNA-sequencing transcriptome and splicing database of glia, neurons, and vascular cells of the cerebral cortex. J Neurosci. 2014; 34:11929–11947. [PubMed: 25186741]

Highlights

- Activation of L-type Ca^{++} channels stimulates oligodendrocyte differentiation.
- Oligodendrocyte proliferation was reduced after L-type Ca^{++} channels knockdown.
- L-type Ca^{++} channels seem to be necessary for oligodendrocyte-neuron interaction.

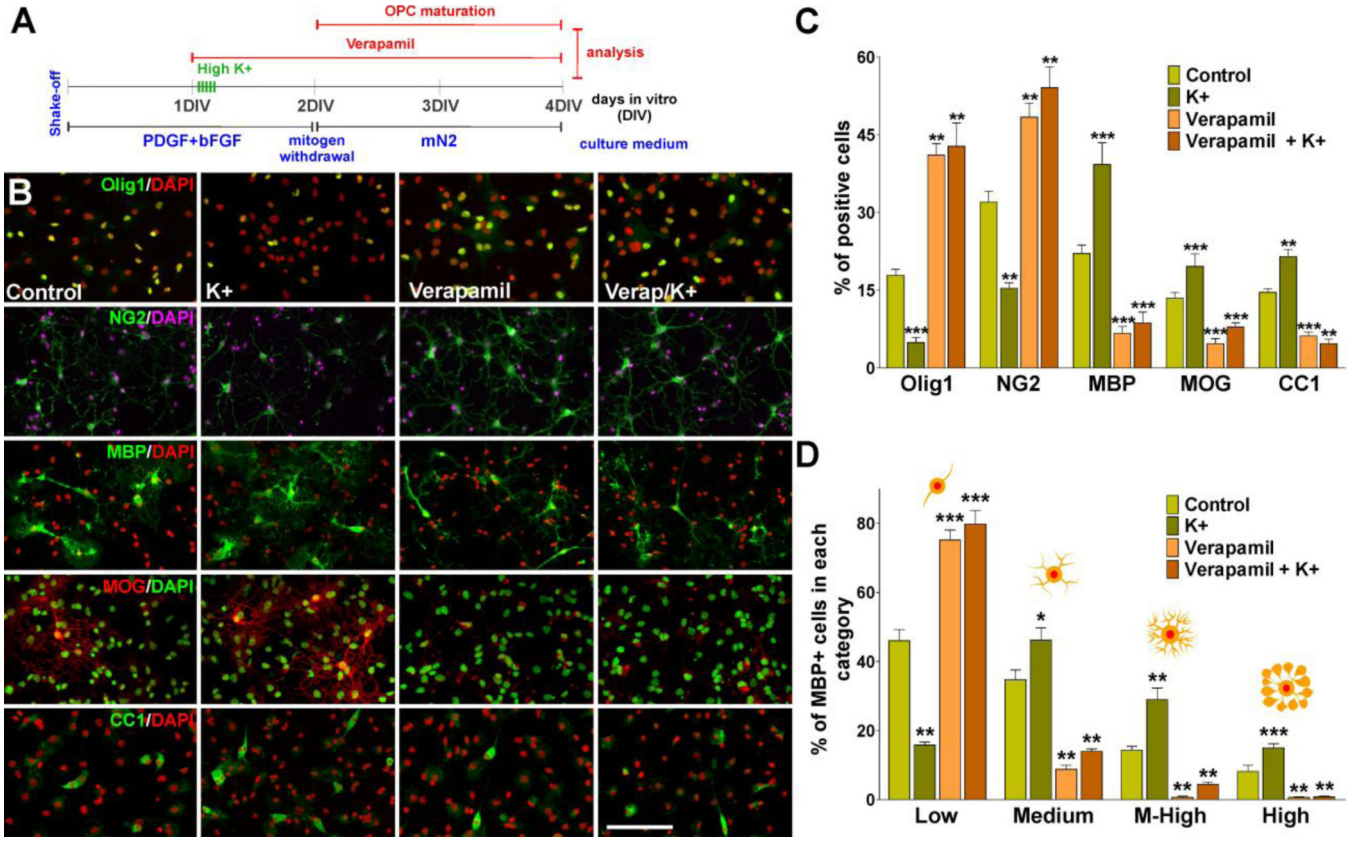

FIGURE 1. L-type VOCC activation stimulates OPC maturation

(**A**) One day after plating, OPCs were treated with high K^+ and the L-type VOCC inhibitor verapamil. Verapamil (5μM) was added to the culture media for three consecutive days and high K^+ (20mM) was applied in five consecutive pulses (5min/each) distributed during the first 5h of the second day in vitro. (**B–C**) After treatment OPCs were stained with antibodies against Olig1, NG2, MBP, MOG and CC1 and the percentage of positive cells in each experimental condition was examined by confocal microscopy. Scale bar = 60μm (Olig1, MOG, CC1); 80μm (NG2, MBP). (**D**) Morphological complexity of MBP-positive cells was scored in four categories. Values are expressed as mean ± SEM of four independent experiments. *p<0.05, **p<0.01, ***p<0.001 vs. respective controls.

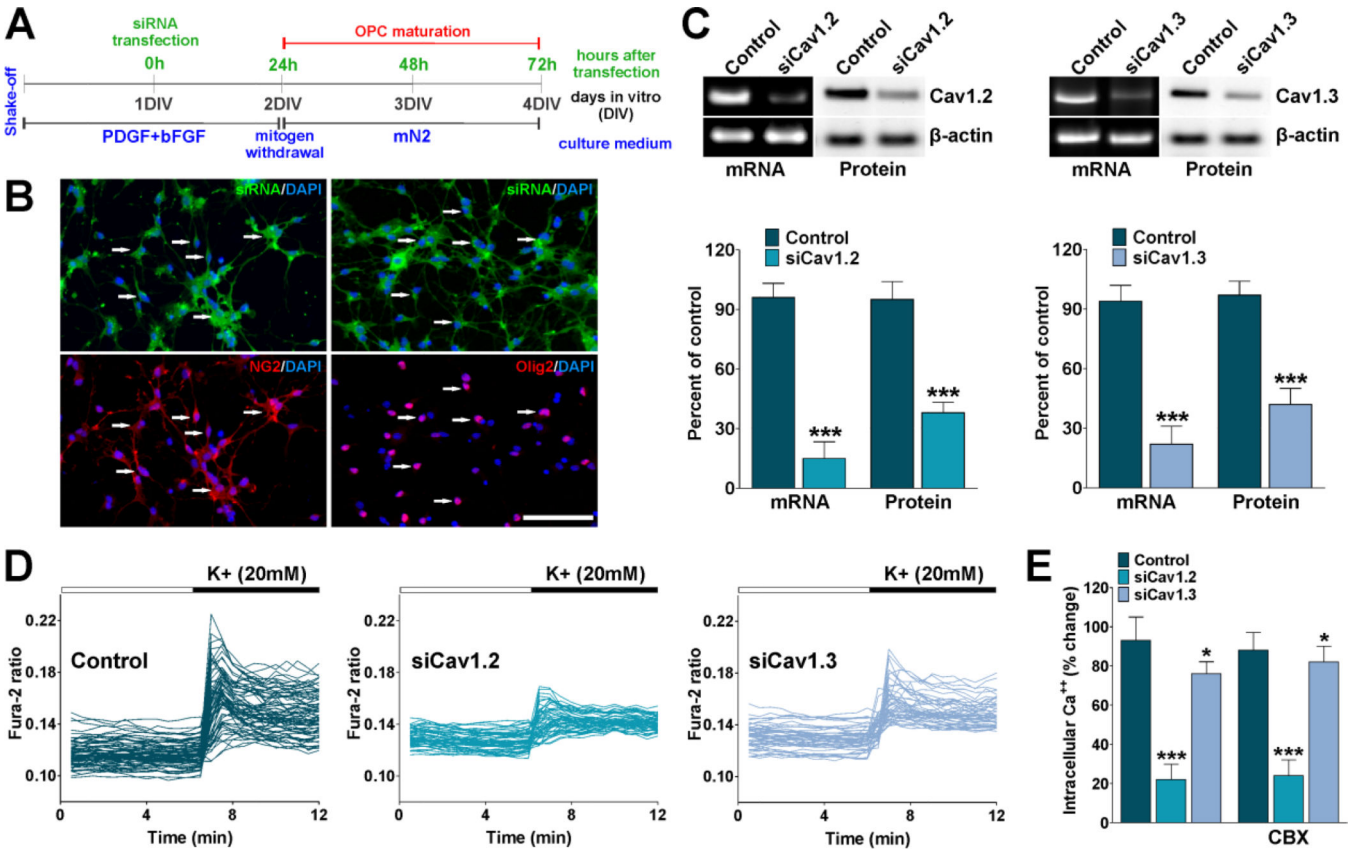

FIGURE 2. siRNA knockdown of L-type VOCCs in OPCs

(**A**) One day after plating, OPCs were transfected with a combination of three different siRNA duplexes specific for Cav1.2 and Cav1.3 (siCav1.2/1.3). After transfection OPCs were further cultured for 24h in defined culture media plus PDGF and bFGF and then induced to exit from the cell cycle and differentiate by switching the cells to a mitogen-free medium (mN2). (**B**) OPCs were treated with fluorescein-labeled dsRNA oligomers to determine siRNA transfection efficiency. 24h after transfection the cells were stained with antibodies against NG2 and Olig2. Scale bar = 80μm. (**C**) 72h after siRNA transfection semi-quantitative RT-PCR and western blot analysis of Cav1.2 and Cav1.3 expression in OPCs was performed using β-actin as internal standard. Data from three independent experiments are summarized based on the relative spot intensities and plotted as percent of controls. (**D**) 72h after siRNA transfection VOCC activity was examined in cultured OPCs using Fura-2 as intracellular Ca^{++} indicator. Note that each trace corresponds to a single cell and the horizontal bars indicate the time of addition of external solution containing high K^{+}. (**E**) The bar graph shows the average amplitude of the Ca^{++} response, calculated from the responding cells expressed as a percentage of change of the emission intensities. The same experiment was performed in the presence of carbenoxolone (200μM) (CBX). Values are expressed as mean ± SEM of at least six independent experiments. *p<0.05, ***p<0.001 vs. control.

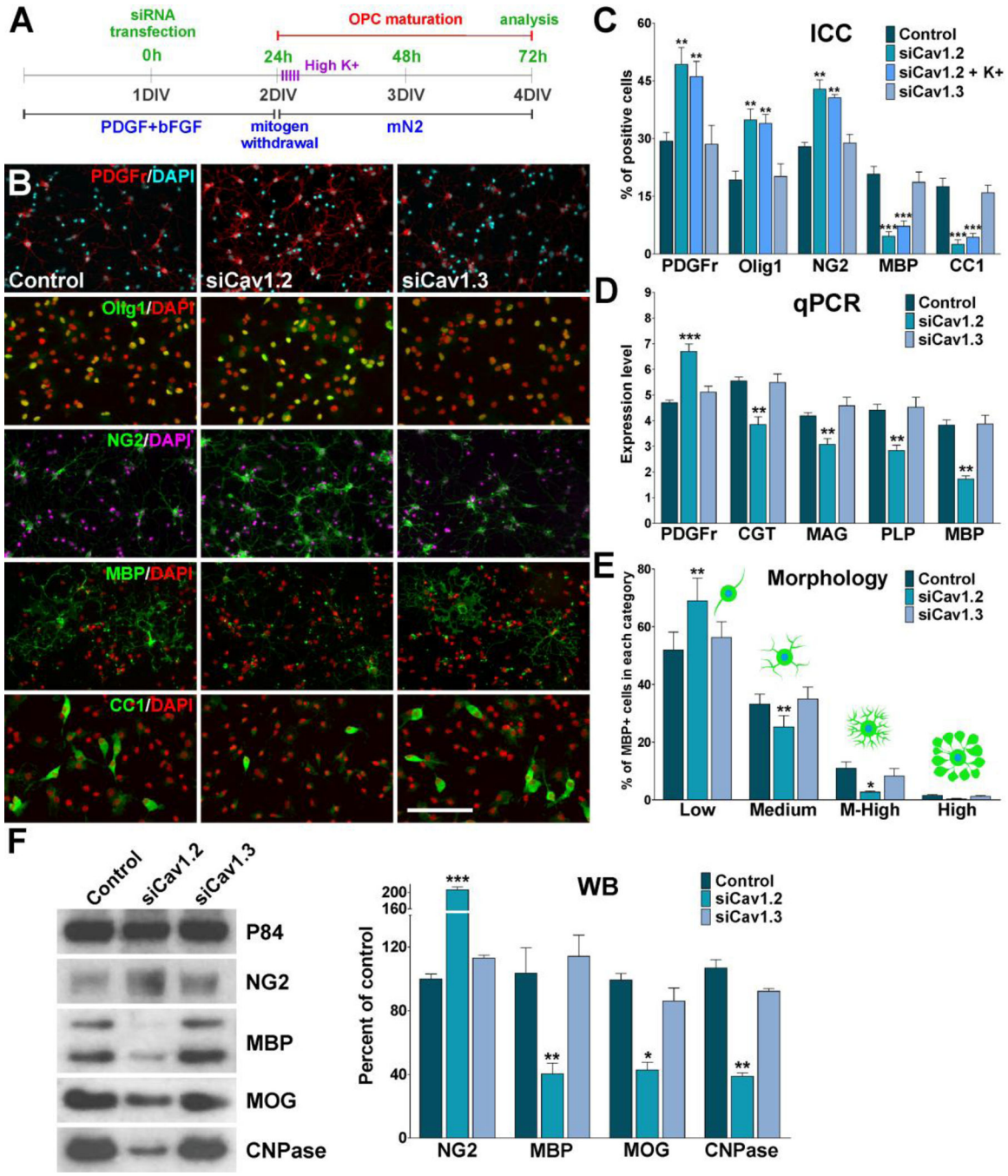

FIGURE 3. Cav1.2 knockdown prevents OPC maturation

(**A**) OPCs were transfected with siRNA duplexes specific for Cav1.2 and Cav1.3 (siCav1.2/1.3) and grown as described in Figure 2. 24h after siRNA transfection, a group Cav1.2 deficient OPCs were treated with high K^+. High K^+ (20mM) was applied in five consecutive pulses (5min/each) distributed during the first 5h of the third day in vitro. (**B–C**) 72h after siRNA transfection, OPCs were stained with antibodies against PDGFr, Olig1, NG2, MBP and CC1 and the percentage of positive cells in each experimental condition was examined by confocal microscopy. Scale bar = 60μm (Olig1, CC1); 80μm (PDGFr, NG2,

MBP). (**D**) Real-time PCR experiments were performed using total mRNA extracted from primary cultures of OPCs and specific primers for PDGFr, CGT, MAG, PLP and MBP (Table II). (**E**) Morphological complexity of MBP-positive cells was scored in four categories. (**F**) Western blot analysis of myelin proteins expression in OPC primary cultures was performed 72h after siRNA transfection using P84 as internal standard. Data from three independent experiments are summarized based on the relative spot intensities and plotted as percent of controls. Values are expressed as mean ± SEM of four independent experiments. *p<0.05, **p<0.01, ***p<0.001 vs. respective controls. **ICC:** Immunocytochemistry, **qPCR**: quantitative real-time PCR, **WB:** Western blot.

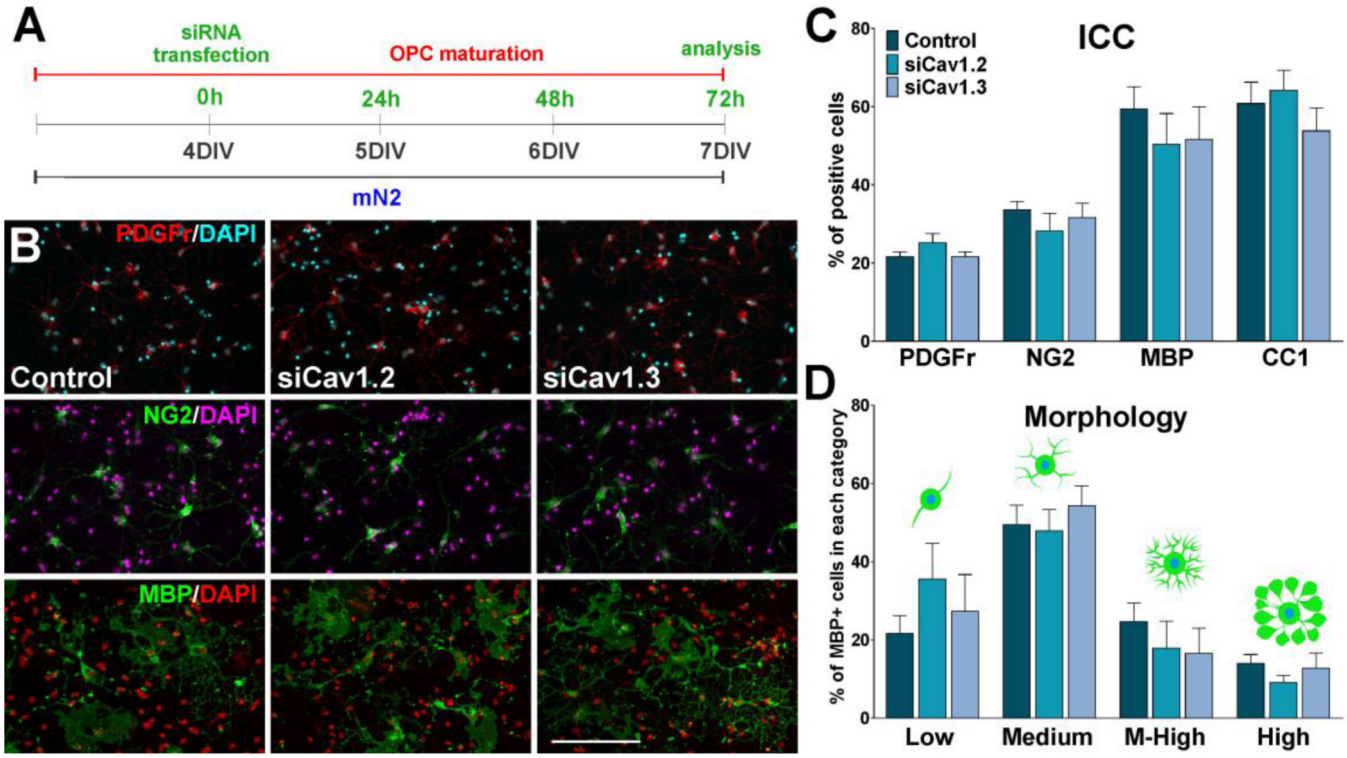

FIGURE 4. Cav1.2 knockdown has no effect on the development of more mature premyelinating oligodendrocytes

(**A**) OPCs were transfected with Cav1.2/1.3 siRNAs after being induced to differentiate by mitogen deprivation. (**B–C**) Premyelinating oligodendrocytes were stained with antibodies against PDGFr, NG2, MBP and CC1 and the percentage of positive cells in each experimental condition was examined by confocal microscopy. Scale bar = 80μm. (**D**) Morphological complexity of MBP-positive cells was scored in four categories. Values are expressed as mean ± SEM of four independent experiments. **ICC:** Immunocytochemistry.

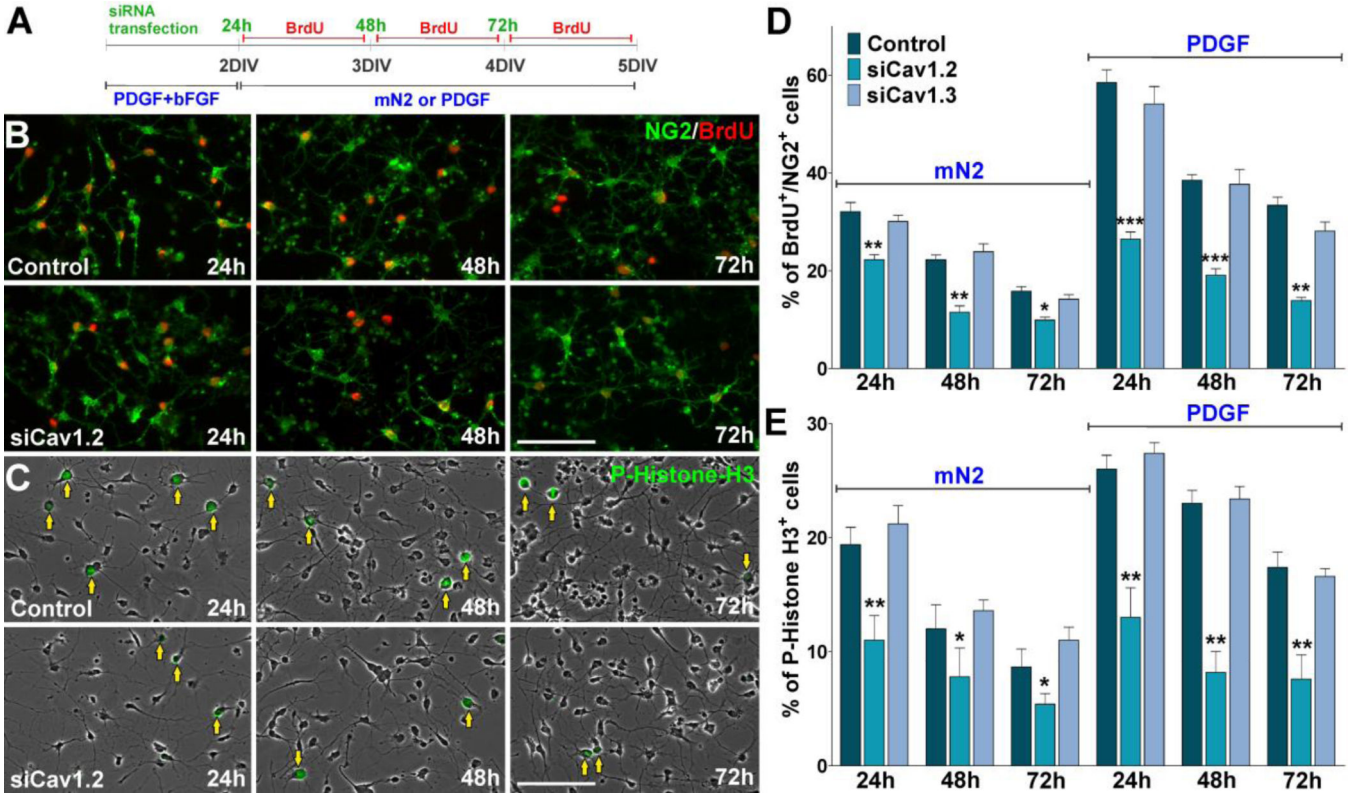

FIGURE 5. Decreased cell division in OPCs lacking Cav1.2

(**A**) OPCs were transfected with siRNA duplexes specific for Cav1.2 and Cav1.3 (siCav1.2/1.3) and grown either in the presence or absence of PDGF. 24h pulses of BrdU were begun at 24h, 48h and 72h after siRNA transfection. After each BrdU pulse, cells were fixed and immunostained with anti-BrdU and anti-NG2 antibodies. (**B–C**) Microphotographs showing $NG2^+/BrdU^+$ and P-Histone $H3^+$ cells grown in mN2 at different time points after siRNA transfection. Arrows indicate P-Histone $H3^+$ cells. Scale bar = 60μm. (**D–E**) The percentage of $NG2^+/BrdU^+$ and P-Histone $H3^+$ cells in each experimental condition was compared with respective controls. Values are expressed as mean ± SEM of four independent experiments. *p<0.05, **p<0.01, ***p<0.001 vs. respective controls.

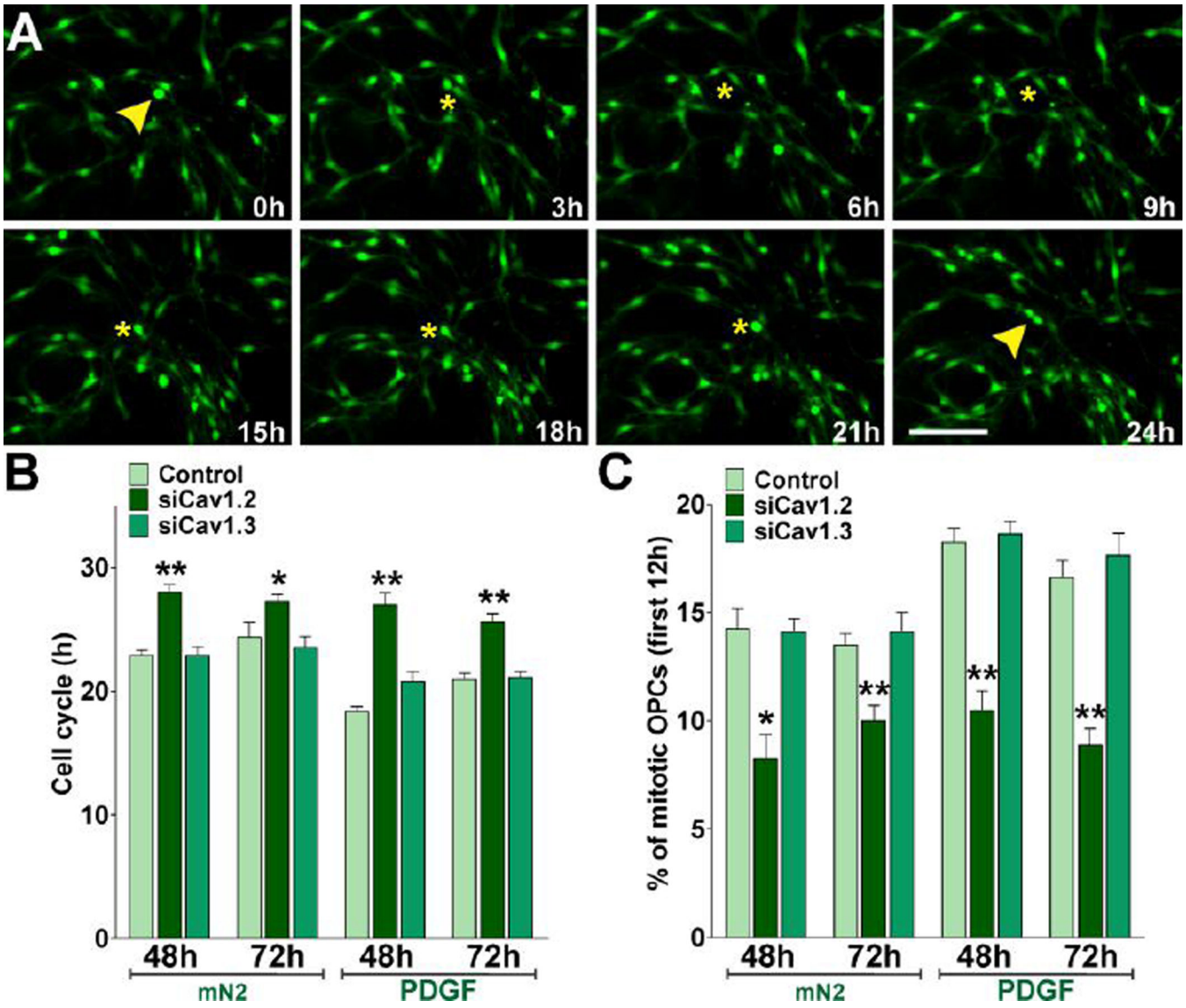

FIGURE 6. Cav1.2 knockdown increases the cell cycle time of mouse OPCs

Primary cultures of PLP-GFP labeled OPCs were transfected with siRNA duplexes specific for Cav1.2 and Cav1.3 (siCav1.2/1.3) and cultured as described in Figure 5. 48h and 72h after transfection, OPCs were incubated in a chamber with 5% CO2 at 37°C, which was placed on the stage of a spinning disc confocal microscope. GFP-labeled OPC clones were imaged with a specific GFP filter at 6min intervals for a period of 30h. (**A**) Time-lapse series of OPCs from control cultures. Yellow arrowheads designate cytokinesis events. Tracking of cells between birth cytokinesis and division cytokinesis was noted with a yellow asterisk near the cell, which was generated from frame to frame. Each frame represents a single section of a time lapse video sequence. Time is denoted in hours in the bottom right corner. Scale bar = 60μm. (**B–C**) Estimated cell cycle times and percentage of mitotic OPCs for each experimental condition. Values are expressed as mean ± SEM of four independent experiments. *p<0.05, **p<0.01, vs. respective controls.

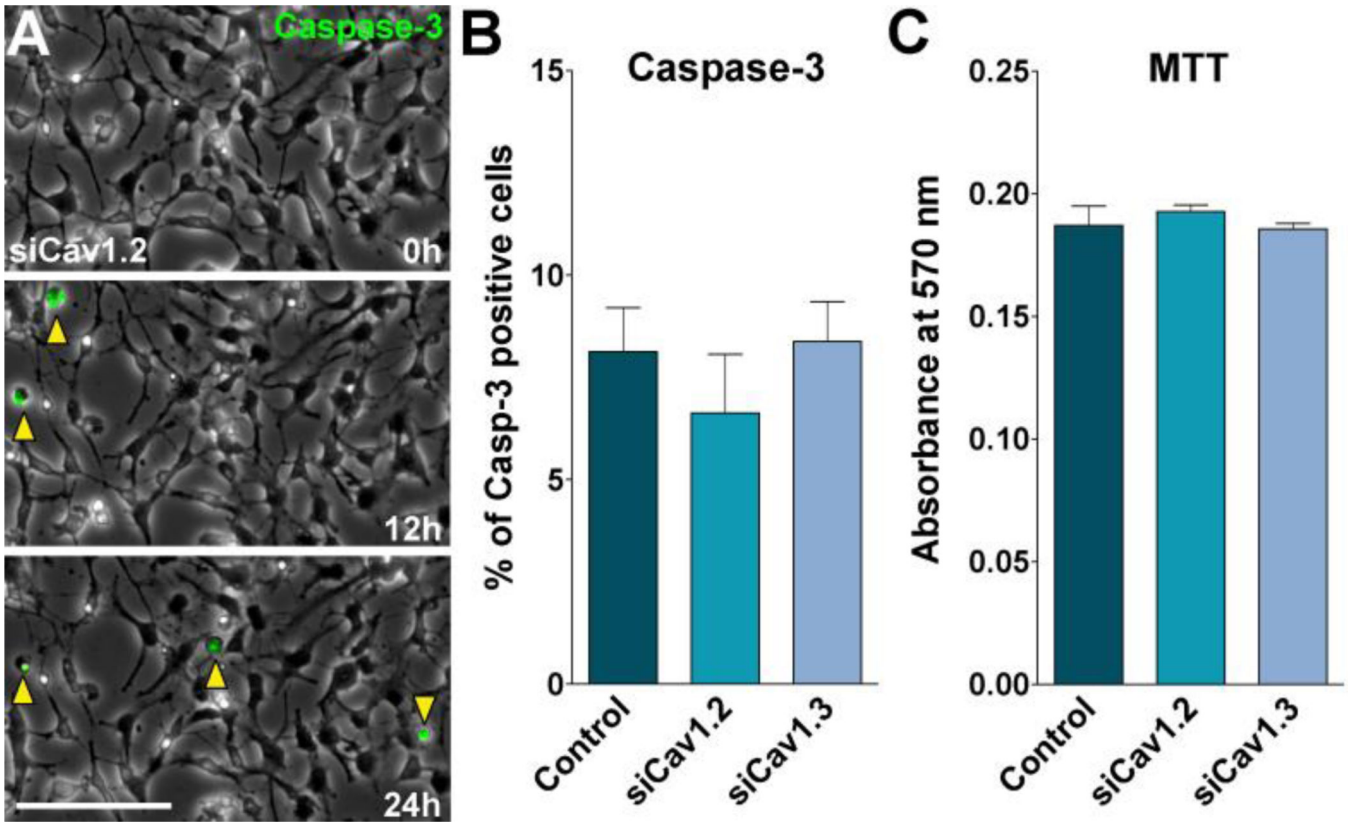

FIGURE 7. OPC viability after L-type VOCC knockdown

OPCs were transfected with siRNA duplexes specific for Cav1.2 and Cav1.3 (siCav1.2/1.3) and grown as described in Figure 2. (**A**) Real-time Caspase-3 assay, using NucView 488 Caspase-3 substrate, was performed as described in Materials and Methods. Fluorescent field images were obtained with a specific GFP filter at 6min intervals for a period of 24h beginning 48h after siRNA transfection. Bright field images were superimposed to show the cell morphology. Yellow arrowheads designate some apoptotic OPCs (Caspase-3^+ cells). Time is denoted in hours in the bottom right corner. Scale bar = 60μm. (**B**) OPCs death were evaluated by measuring the percentage of Caspase-3^+ cells in each experimental group for a period of 24h. (**C**) Evaluation of OPCs viability by the MTT assay 48h after siRNA transfection. Values are expressed as mean ± SEM of five independent experiments.

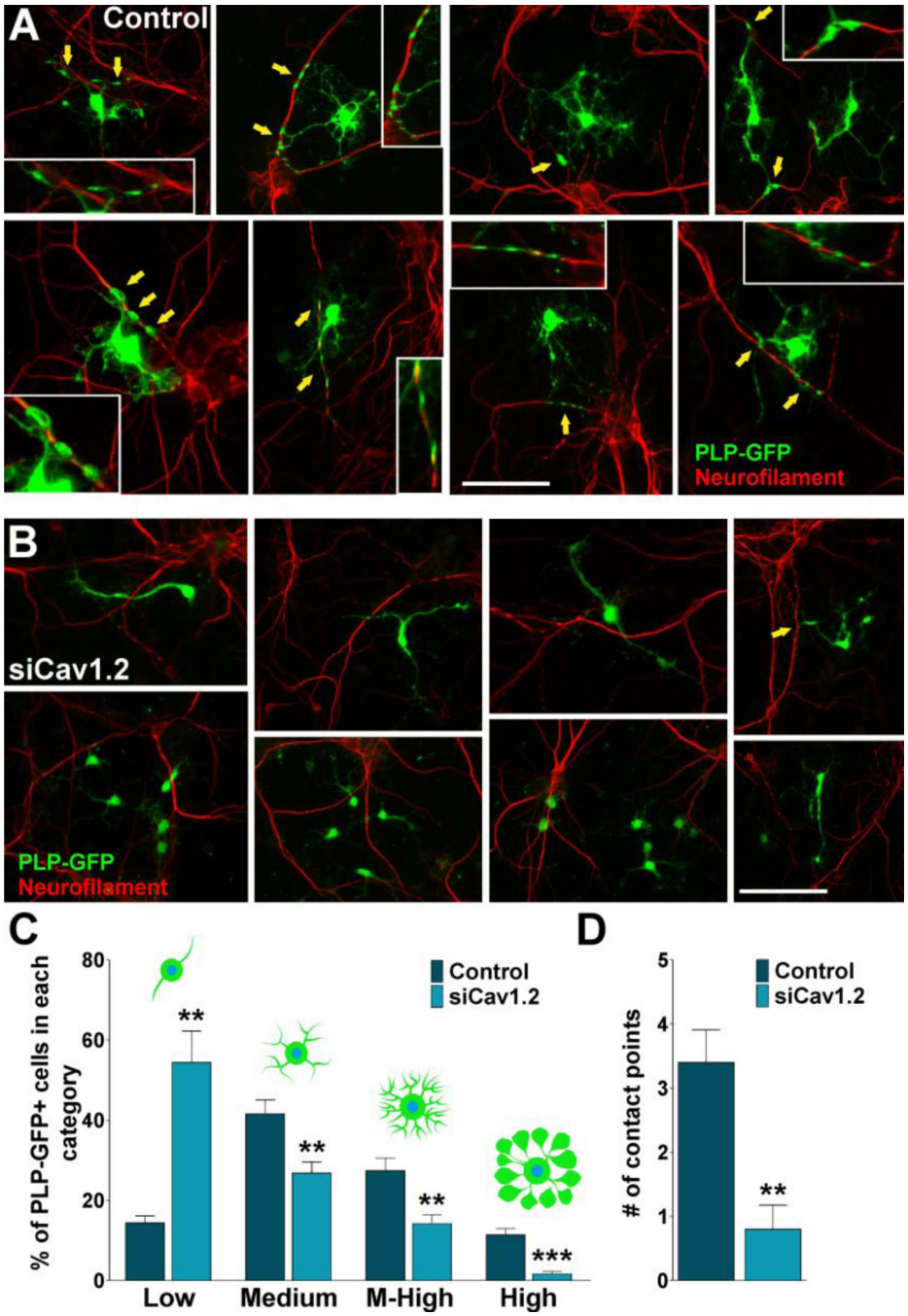

FIGURE 8. Co-culture of cortical neurons and VOCC deficient OPCs

(**A–B**) PLP-GFP labeled OPCs were transfected with siRNA duplexes specific for Cav1.2 (siCav1.2). 24h after siRNA transfection, control and transfected OPCs were co-cultured with cortical neurons for 7 days. Arrows indicate oligodendrocyte-neurite contact points (see insets for high magnification pictures). Scale bar = (A) 60μm; (B, upper panel) 60μm, (B, lower panel) 80μm. (**C**) Morphological complexity of control and siCav1.2 transfected PLP-GFP^{+} cells in co-culture was scored in 4 categories. (**D**) The number of contact points with neurites was analyzed in control and Cav1.2 transfected cells. Results are the means ± SEM

for three independent experiments. >200 cells were analyzed per experimental condition.**p<0,01 and ***p<0,001 vs. respective controls.

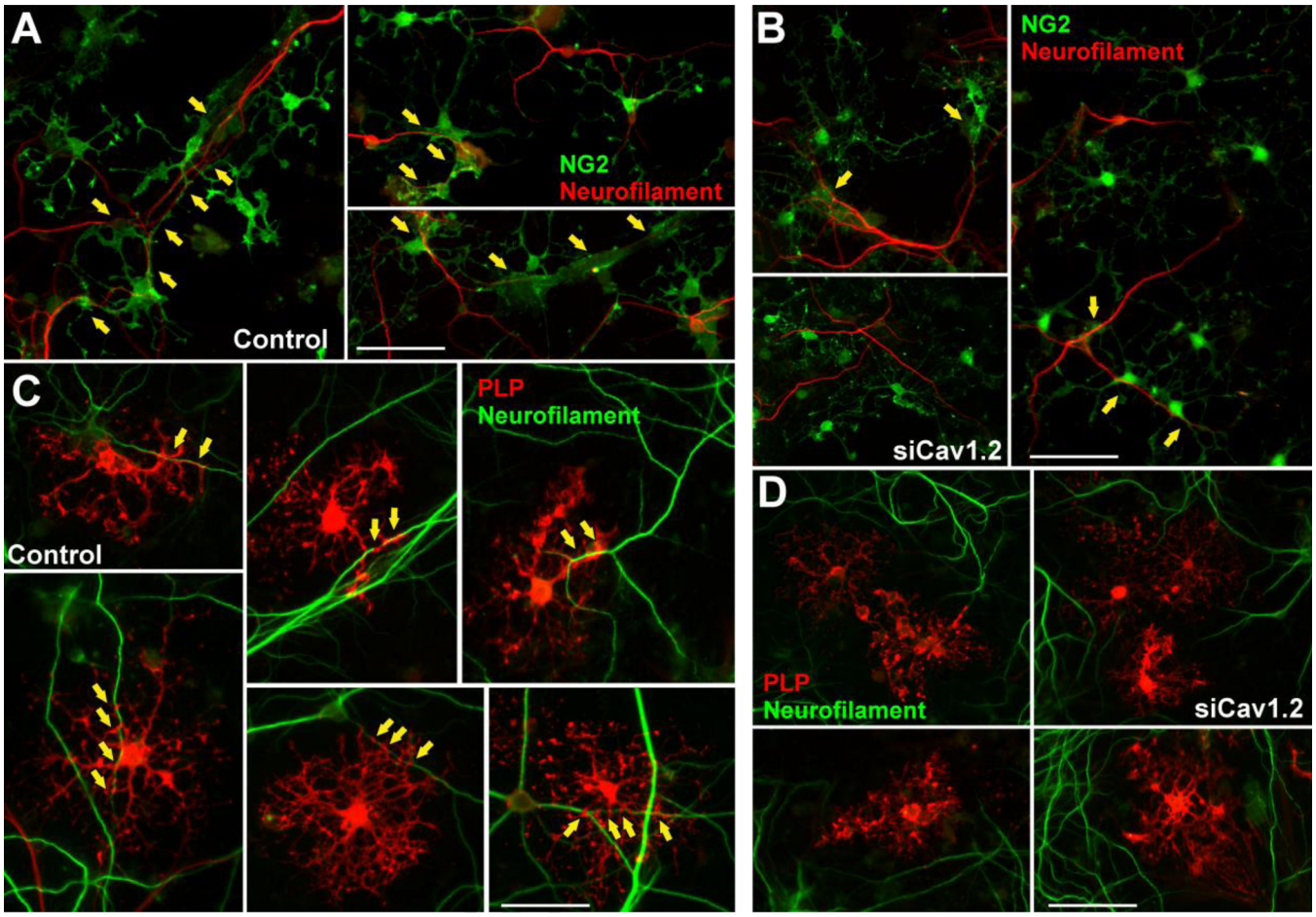

FIGURE 9. VOCC deficient oligodendrocytes fail to interact with neurons at different developmental stages

OPCs were transfected with siRNA duplexes specific for Cav1.2 (siCav1.2). 24h after siRNA transfection, control and transfected OPCs were co-cultured with cortical neurons for 7 days. (**A–B**) Examples of NG2 immunostaining in 7 days old co-cultures. Scale bar = (A) 40μm; (B) 60μm. (**C–D**) Examples of PLP immunostaining in 7 days old co-cultures. Scale bar = 40μm. Yellow arrows indicate oligodendrocyte-neurite contact points.

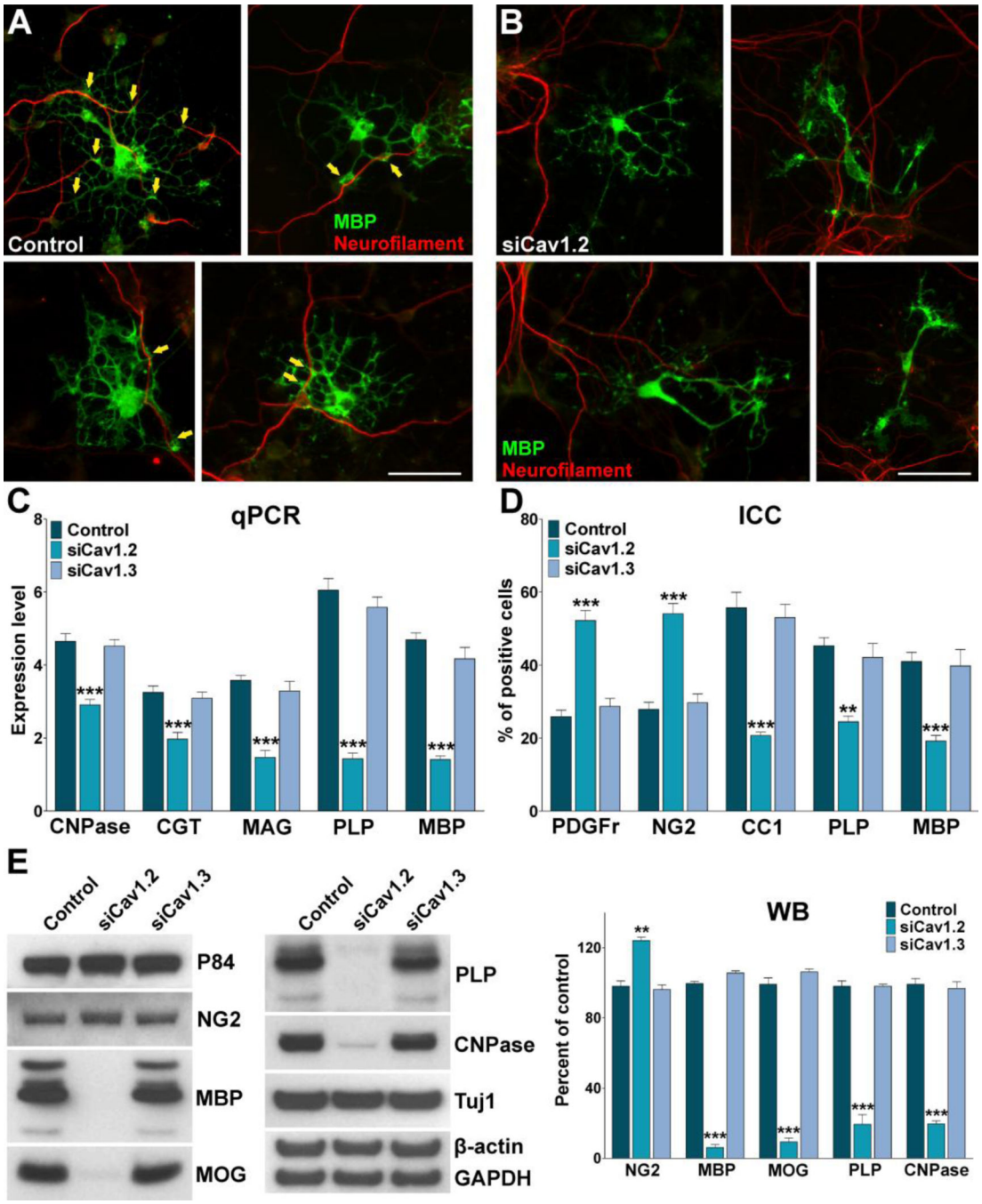

FIGURE 10. L-type VOCCs are necessary for neuron-glia interaction and myelination in vitro

Co-cultures were prepared as described in Figure 9. (**A–B**) Examples of MBP immunostaining in 7 days old co-cultures. Scale bar = 40μm. Yellow arrows indicate oligodendrocyte-neurite contact points. (**C**) Real-time PCR experiments were performed using total mRNA extracted from 7 days old co-cultures and specific primers for CNPase, CGT, MAG, PLP and MBP (Table II). (**D**) Immunocytochemical analysis of oligodendrocyte differentiation markers and myelin protein expression in 7 days old co-cultures. OPCs were stained with antibodies against PDGFr, NG2, CC1, PLP and MBP and

the percentage of positive cells in each experimental condition was examined by confocal microscopy. (**E**) Western blot analysis of myelin proteins expression in 7 days old co-cultures was performed using P84, GAPDH and β-actin as internal standards. Data from three independent experiments are summarized based on the relative spot intensities and plotted as percent of controls. Values are expressed as mean ± SEM of four independent experiments. **p<0.01, ***p<0.001 vs. respective controls. **ICC:** Immunocytochemistry, **qPCR**: quantitative real-time PCR, **WB:** Western blot.

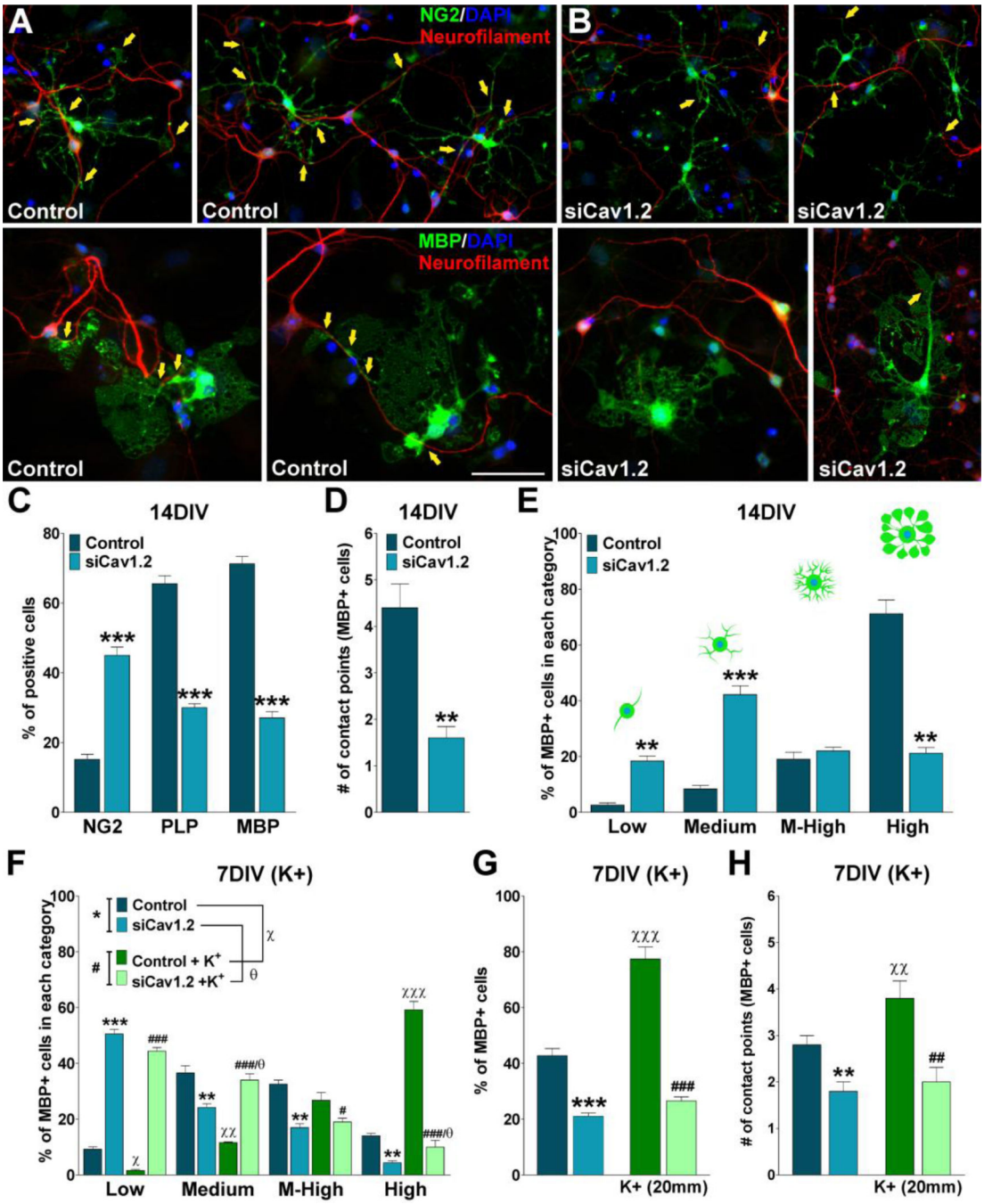

FIGURE 11. Two weeks of co-culture did not significantly improve the maturation of OPCs lacking L-type VOCCs

Co-cultures were prepared as described in Figure 9. (**A–B**) Examples of NG2 and MBP immunostaining in 14 days old co-cultures. Scale bar = (NG2) 60μm; (MBP) 40μm. Yellow arrows indicate oligodendrocyte-neurite contact points. (**C**) Percentage of NG2, PLP and MBP positive cells in 14 days old co-cultures. (**D**) The number of contact points with neurites was analyzed in control and siCav1.2 MBP$^+$ cells. (**E**) Morphological complexity of control and siCav1.2 MBP$^+$ cells was scored in 4 categories. Co-cultures were treated with

high K^+. Potassium was applied in three consecutive pulses (5min/each) distributed during the first 3h of the second, third and fourth day in vitro. After treatment, the morphological complexity (**F**), the percentage (**G**) and the number of contact points with neurites (**H**) of MBP^+ cells was analyzed in each experimental condition. Values are expressed as mean ± SEM of four independent experiments. *p<0.05, **p<0.01, ***p<0.001 vs. respective controls.

Table I

Sequences of Stealth RNAi™ siRNA duplexes used for Cav1.2 and Cav1.3 knockdown.

		siRNA Duplex Oligoribonucleotides Sequence
Cav1.2	**siRNA1**	GCCAUGAAUAUACUCAACAUGCUUU
		AAAGCAUGUUGAGUAUAUUCAUGGC
	siRNA2	UGAUGUCAUUCUCAGUGAGACUAAU
		AUUAGUCUCACUGAGAAUGACAUCA
	siRNA3	AGGCAGCAUGGAAGCUCAGCUCUAA
		UUAGAGCUGAGCUUCCAUGCUGCCU
Cav1.3	**siRNA1**	GCCAUGAGAGAUAACAACCAGAUCA
		UGAUCUGGUUGUUAUCUCUCAUGGC
	siRNA2	CCUCCAGCUGGUGAUGAUGAGGUAA
		UUACCUCAUCAUCACCAGCUGGAGG
	siRNA3	CGUAUGGACUGUUGCUGCAUCCUAA
		UUAGGAUGCAGCAACAGUCCAUACG

Table II

Sequences of primers used for real-time PCR

Gene	Forward	Reverse
PDGFr	5’-TCTCACTGAGATCACCACCGA	5’-CGCTGTCTTCTTCCTTAGCC
MAG	5’-GGTGTTGAGGGAGGCAGTTG	5’-CGTTGTCTGCTAGGCAAGCA
CGT	5’-TGCCAACGTATCCTTCTTCC	5’-CATTGTCCCATGTCAAGCAC
CNPase	5’-AACCAATGGCAGCTGTCG	5’-TCAGGAACCAGCCAAAGTAAA
PLP	5’-CCCACCCCTCTCCGCTAGTT	5’-CAGGAAAAAAAGCACCATTGTG
MBP	5’-CATTACTTAGTGCCAATTAGGTTC	5’-GTCAGTCGTCTTGTTACTCTAC
GAPDH	5’-ACTCCACTCACGGCAAATTC	5’-TCTCCATGGTGGTGAAGACA